Nonlinear Dyn (2011) 63: 561–586
DOI 10.1007/s11071-010-9820-5

ORIGINAL PAPER

Improved reduced order solution techniques for nonlinear systems with localized nonlinearities

I.R. Praveen Krishna · C. Padmanabhan

Received: 21 October 2009 / Accepted: 18 August 2010 / Published online: 11 September 2010
© Springer Science+Business Media B.V. 2010

Abstract This paper examines the modeling and solution of large-order nonlinear systems with continuous nonlinearities which are spatially localized. This localization is exploited by a combined component mode synthesis (CMS)—dynamic substructuring approach for efficient model reduction. A new ordering method for the Fourier coefficients used in the Harmonic Balance Method (HBM) is proposed. This allows the calculation of the slave dynamic flexibility matrix, using simple analytical expressions thus saving considerable computational effort by avoiding inverse calculation. This procedure is also capable of handling proportional damping. A hypersphere-based continuation technique is used to trace the solution, and hence track bifurcations since it has the advantage that the augmented Jacobian matrix remains square. The reduced system is also solved using a time-variational method (TVM) which generates sparse Jacobian matrices when compared with HBM. Several systems including those with parametric excitation and internal resonances are solved to demonstrate the capability of the proposed schemes. A comparison of these techniques and their effectiveness in solving extremely strong nonlinear systems with continuous nonlinearities is discussed.

I.R. Praveen Krishna · C. Padmanabhan (✉)
Machine Design Section, Department of Mechanical Engineering, Indian Institute of Technology Madras, Chennai 600036, India
e-mail: mouli@iitm.ac.in

Keywords Large nonlinear systems · Mode superposition · Dynamic condensation · Component mode synthesis · Harmonic balance · Time variational method · QR · LU · SVD · Powell hybrid method · Continuation · Hypersphere

Nomenclature

HBM	Harmonic Balance Method
TVM	Time Variational Method
DOF	Degrees-of-Freedom
$\mathbf{M}$	Mass matrix
$\mathbf{C}$	Damping matrix
$\mathbf{K}$	Stiffness matrix
$\ddot{\mathbf{x}}$	Acceleration vector
$\dot{\mathbf{x}}$	Velocity vector
t	Time
$\mathbf{x}$	Displacement vector
$\mathbf{f}(\mathbf{x}, \dot{\mathbf{x}})$	Nonlinear force vector
$\mathbf{F}(\mathbf{t})$	External excitation vector
$\mathbf{x}_k(\mathbf{t})$	Approximated Fourier series expansion of displacement vector for kth *DOF*
$\tilde{x}_{k0}$	DC term of the Fourier series expansion of displacement kth *DOF*
$\tilde{x}^c_{kn}$	Coefficient of the cosine term of Fourier series expansion of displacement kth *DOF*
$\tilde{x}^s_{kn}$	Coefficient of the sine term of Fourier series expansion of displacement kth *DOF*
$\mathbf{F}_k(\mathbf{t})$	Approximated Fourier series expansion of external force vector applied on kth *DOF*

$\tilde{F}_{k0}$	DC term of the Fourier series of external force vector kth *DOF*
$\tilde{F}^c_{kn}$	Coefficient of the cosine term of Fourier series of external force vector kth *DOF*
$\tilde{F}^s_{kn}$	Coefficient of the sine term of Fourier series expansion of external force vector kth *DOF*
$\mathbf{f}_k(\mathbf{x}, \dot{\mathbf{x}})$	Approximated Fourier series expansion of nonlinear force vector kth *DOF*
$\tilde{f}_{k0}$	DC term of the Fourier series of expansion of nonlinear force vector kth *DOF*
$\tilde{f}^c_{kn}$	Coefficient of the cosine term of Fourier series of nonlinear force vector kth *DOF*
$\tilde{f}^s_{kn}$	Coefficient of the sine term of Fourier series expansion of nonlinear force vector kth *DOF*
$\mathbf{f}_{pk}(\mathbf{x}, \dot{\mathbf{x}}, \mathbf{t})$	Approximated Fourier series expansion of parametric excitation vector kth *DOF*
$\tilde{f}_{pk0}$	DC term of the Fourier series of expansion of parametric excitation vector kth *DOF*
$\tilde{f}^c_{pkn}$	Coefficient of the cosine term of Fourier series of parametric excitation vector kth *DOF*
$\tilde{f}^s_{pkn}$	Coefficient of the sine term of Fourier series expansion of parametric excitation vector kth *DOF*
α	Nonlinear/Parametric excitation coefficient
$\mathbf{R}(\gamma)$	Residue vector
$\mathbf{Y}$	Fourier/ Time variational Admittance Matrix
$\mathbf{Y}_s s^{-1}$	Slave Flexibility Matrix
$\mathbf{J}$	Jacobian matrix
ϵ	Convergence tolerance
$\hat{\mathbf{f}}$	Nonlinear force TVM coefficients
$\hat{\mathbf{x}}$	Displacement TVM coefficients
$\hat{\mathbf{F}}$	External force TVM coefficients
$\mathbf{U}$	Eigen vector matrix
$\boldsymbol{\phi}$	Retained Mode matrix
$\boldsymbol{\psi}$	Constraint mode matrix
ζ	Damping ratio
ω	Excitation frequency
Ω_i	ith Natural frequency
Δ	Increment between iterations
c	Hypersphere center
FM	Full Model
MS	Mode Superposition
PC	Physical Condensation
CM	Component Mode

Subscripts

ss	Slave partition
sm	Slave master partition
ms	Master slave partition
mm	Master master partition

1 Introduction

The nonlinearities in a significant number of mechanical systems are localized. For example, squeeze film dampers in a rotor-bearing system, rubbing between the stator and rotor of gas turbine engines or interface friction in turbine blades which generate nonlinear forces are localized spatially. The mathematical models for most of the above described mechanical systems are developed using finite element techniques with the resulting model size of the order of at least a few thousands of degrees-of-freedom (DOF). Out of these few thousand DOF, only very few will be nonlinear DOF for the class of problems described above. Hence, it is a waste of storage and computational time if the traditional nonlinear solution techniques are applied to all the DOF.

The reduction of model size for dynamic analysis is well known in the case of linear systems. Most of the commercial finite element packages use mode superposition techniques for harmonic as well as transient response calculations. The modal truncation error is minimized by the use of mode acceleration method or mode-displacement method. Other methods for the model size reduction are static or dynamic condensation. The condensation idea was first developed by Guyan [1]. He used only static condensation for reducing the system. Leung and Fung [2] extended the dynamic sub-structuring technique to both linear and nonlinear systems. The dynamic flexibility matrix is expanded in terms of the fixed interface natural modes of the system. They used the condensed dynamic stiffness matrix as a function of the excitation frequency and reduced the problem to only the nonlinear coordinates. In his book, Qu [3] describes many methods for the static and dynamic condensation.

Another commonly used method for the dynamic analysis of the large structures is the component mode

synthesis originally proposed Hurty [4] and then modified by Craig and Bampton [5]. Here, a complex structure is divided into distinct regions, or substructures. Using modal truncation along with the geometric compatibility condition, a reduced model is built for the complete structure. Another model reduction procedure is based on the Krylov subspace method [6]. Here, the linear system is solved iteratively avoiding matrix–matrix multiplications but using matrix–vector multiplications.

Since the nonlinear system does not obey the principle of superposition, its treatment requires entirely different methods of solution. There are basically two approaches to handle a nonlinear problem. First is a qualitative technique concerned with the general behavior and stability of the system near the neighborhood of a known solution, and second quantitative techniques to find the solution to the differential equations developed from the nonlinear system, which may not be available in closed form unlike linear theory. The theory of nonlinear equations relies highly on the approximations derived from the linear theory and such approximations can be applied directly to the nonlinear terms in the neighborhood of a fixed point or an orbit. These approaches are usually grouped as perturbation approaches with the strength of the nonlinearity being small; hence it cannot be applied to strongly nonlinear systems. Another approach generally used by the nonlinear community is time integration of the governing differential equations based on standard numerical methods [7, 8]. Generally, they are computationally expensive as one has to start from a set of initial conditions and then proceed in time until the transients attenuate due to system damping and a steady state response is finally obtained. The time involved increases as the size of the model is increased and if one has to chart out the multiple solutions likely for a set of design parameters, then a large initial condition map is required. Another disadvantage of the numerical integration process is the "stiffness" of the system (i.e., the condition number of the state space matrix). If the system is too stiff then methods such as Backward Difference Formula (BDF) are used, which are computationally more intensive than traditional numerical integration methods.

A class of semianalytical procedures has been developed for the analysis of the nonlinear systems, subjected to periodic excitation, using basis functions in the time domain [9], frequency domain, or alternating between both domains. Then the system is minimized in a weighted residual sense using a variational approach. The main advantage of these methods is that they are computationally less intensive than numerical integration. Urabe and Reteir [10] were the first to formulate a Galerkin-based harmonic balance method. The issues of convergence and uniqueness were addressed by them. In the following years, a number of papers appeared with varying nomenclature such as incremental harmonic balance method, trigonometric collocation method, and Alternating Frequency-Time (AFT) analysis [11–16]. But most of these techniques are essentially similar in principle. Cameron and Griffin [17] used this principle for the study of a friction damper model subject to a three frequency excitation. Blankenship and Kahraman [18] used the harmonic balance method to find the steady state forced response of a mechanical oscillator with parametric excitation and clearance type nonlinearity. Steady state response of a nonlinear system was found using the harmonic balance method by Leung and Fung [2], but the effect of damping was neglected in their analysis. They included damping for linear substructures in another work [19].

Borri et al. [20] gave a comprehensive review of the basic theory concerned with finite elements in time for dynamics. Wang [21] proposed a finite element in time method for analyzing the periodic stick-slip motion of a SDOF model of frictionally damped turbine blades. Later [22] he studied the dynamic response and stability of a SDOF with unsymmetric piecewise linear nonlinear stiffness using finite element in time. Rook [23] developed a variational approach which permits the calculation of the steady-state time domain response of nonlinear ordinary differential equations. Here, the transients are avoided unlike numerical integration, and unlike harmonic balance all calculations are performed in the time domain. Though he developed a framework for the solution of a multi-DOF system, the examples used were only single DOF systems.

Most of these approximation methods yield a set of nonlinear algebraic equations after transformation and the major computational cost comes from the iterative solution of these algebraic equations. The common method used is the Newton–Raphson method and it has the advantage of quadratic convergence when the initial guess is in the vicinity of the actual solution. For a strongly nonlinear system, this usually becomes difficult, and hence the Newton method may fail. Another

method generally used for solving these equations are based on the quasi-Newton method or variations of the same. Broyden [24] was the first person to propose this method and this class of methods avoid computation of the Jacobian which is required for the Newton–Raphson procedure. The Jacobian is calculated or approximated using finite difference and updated during iteration by an approximation method. One such method called the Powell hybrid method [25] along with a line search algorithm has been reported to be quite robust for the solution of the nonlinear algebraic equations.

Regular numerical integration methods or the time/frequency methods without continuation will not trace the unstable solution branch during the solution phase. Here, in this paper, a hypersphere based approach [26] is used for tracing the entire solution curve (stable as well as unstable). The main advantage of this method is that the resulting Jacobian is a square matrix, and hence the solution is straightforward and more accurate than a rectangular Jacobian generated by regular homotopy/arc-length method, for which a pseudo-inverse is required [27, 28].

Even though different methods have been proposed by different authors for the solution of large systems, the convergence properties of these techniques as a function of strength of the nonlinear parameter(s) are rarely reported in the literature. Comparison between different techniques are also not available in the literature. In this paper, different model reduction techniques such as mode superposition, dynamic condensation, and CMS are used along with HBM and TVM. Even though a dynamic condensation technique is used to reduce the size of the dynamical system using above mentioned methods, the major disadvantage of this method is the fact that at each iteration level the frequency dependent slave system has to be inverted and that becomes an additional computational burden. This can be successfully eliminated without compromising the accuracy in the frequency domain method (HBM) by component mode- based dynamic condensation. A time domain approach for a multi-DOF system using hat function as a basis function is developed and implemented for MDOF systems. The different solution methods for the Newton iteration using LU, QR, and SVD [29] are compared in this paper and their usefulness is also discussed. A quasi-Newton method called the Powell hybrid method along with a line search algorithm is also used for the solution of the nonlinear algebraic equations. Results from both techniques are verified with those from numerical integration (Runge–Kutta–Fehlberg scheme). Numerical integration is also carried out on the reduced model using mode superposition. All the above methods are coupled with the continuation algorithm based on the hypersphere.

2 Model

Six different models are considered for the analysis, two distinct 3 DOF models, an axially vibrating beam, a beam undergoing bending vibration, an internal resonance problem, and a beam with a spring, whose stiffness is time-varying, attached at one end. A cubic nonlinear stiffness is attached to mass m_1 along with the linear stiffness for the first lumped parameter model as shown in Fig. 1 and to mass m_3 for the system shown in Fig. 2. In the case of the axial or beam bending problem or for the parametric excitation problem, the nonlinear stiffness/time-varying stiffness is attached to the free end as shown in Fig. 3. For the 3 DOF models, the external force is applied on the mass to which the nonlinear spring is attached. The model details for the 3 DOF models are given in Table 1. Since the mass, damping, and stiffness matrix are symmetric, only the upper triangular values are given. The axial, beam bending vibration, and the parametric excitation problem has been modeled using standard finite element method and the details regarding the model are shown in Table 2. The damping for the beam is assumed to be proportional. For simulating the internal

Fig. 1 3 DOF model 1

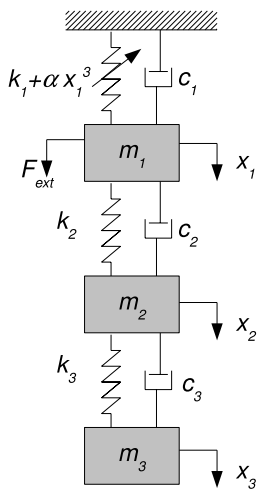

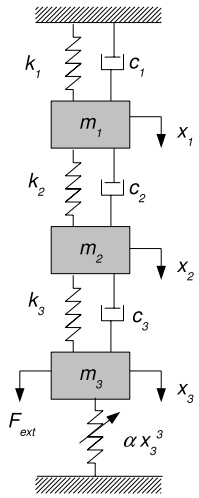

Fig. 2 3 DOF model 2

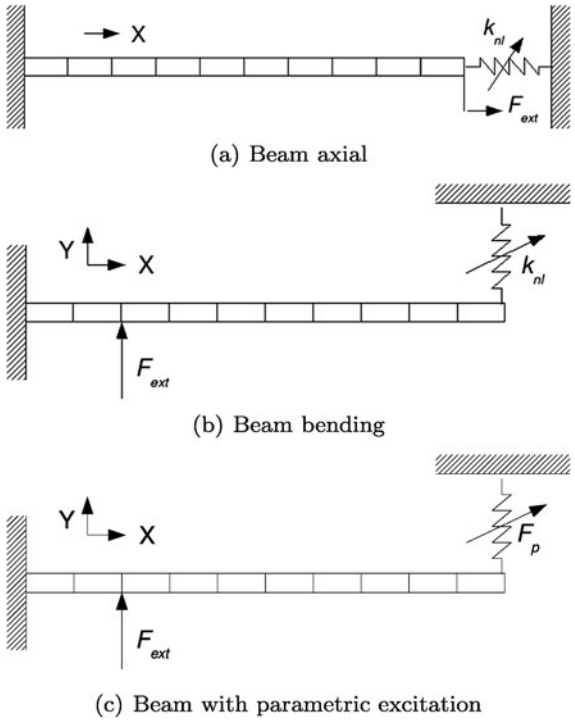

Fig. 3 Beam Axial, Bending, and with parametric excitation

resonance problem, a 9 DOF model is created with repeated eigenvalues as shown in Fig. 4. The model details are given in Table 3. The equations of motion of for all the models considered can be written as

$$\mathbf{M}\ddot{\mathbf{x}} + \mathbf{C}\dot{\mathbf{x}} + \mathbf{K}\mathbf{x} + \mathbf{f}_{\mathrm{p}}(\mathbf{x}, \dot{\mathbf{x}}, \mathbf{t}) + \mathbf{f}(\mathbf{x}, \dot{\mathbf{x}}) = \mathbf{F}_{\mathrm{ext}}(\mathbf{t}), \quad (1)$$

where $\mathbf{M}$, $\mathbf{C}$, and $\mathbf{K}$ are the mass, damping, and stiffness matrix of size $N \times N$, $\mathbf{f}(\mathbf{x}, \dot{\mathbf{x}})$ is the nonlinear function of size $N \times 1$, $\mathbf{f}_{\mathrm{p}}(\mathbf{x}, \dot{\mathbf{x}}, \mathbf{t})$ is the localized parametric excitation force defined in displacement, velocity (or both), and in time, of size $N \times 1$. $\mathbf{x}, \dot{\mathbf{x}}$ and $\ddot{\mathbf{x}}$ are the displacement, velocity, and acceleration vectors, each of size $N \times 1$, $\mathbf{F}_{\mathrm{ext}}(\mathbf{t})$ is the external excitation force vector of size $N \times 1$.

3 Model reduction

3.1 Mode superposition

Let $\mathbf{U}_R$ and $\mathbf{U}_L$ be the right and left eigenvectors of the linear system (system assumed unsymmetrical but with real eigenvalues) containing only the first m modes. The physical coordinates $\mathbf{x}$ is transformed to generalized coordinates $\mathbf{z}$ by $\mathbf{x} = \mathbf{U}_R\mathbf{z}$. Premultiplying the entire equation with $\mathbf{U}_L^T$ yields

$$\mathbf{U}_L^T\mathbf{M}\mathbf{U}_R\ddot{\mathbf{z}} + \mathbf{U}_L^T\mathbf{C}\mathbf{U}_R\dot{\mathbf{z}} + \mathbf{U}_L^T\mathbf{K}\mathbf{U}_R\mathbf{z} + \mathbf{U}_L^T\mathbf{f}_{\mathrm{p}}(\mathbf{z}, \dot{\mathbf{z}}, \mathbf{t}) + \mathbf{U}_L^T\mathbf{f}(\mathbf{z}, \dot{\mathbf{z}}) = \mathbf{U}_L^T\mathbf{F}(\mathbf{t}). \quad (2)$$

The above equation will be of the size $m \times m$ which is sufficiently smaller than the original size N. If the system is symmetric (as is the case with all the examples considered in this paper), then the left and right eigenvectors are the same, i.e., $\mathbf{U}_L = \mathbf{U}_R$. The frequency is normalized to $\Omega = \omega/\omega_n$, where ω_n is the first natural frequency of the system and the time variable is nondimensionalized by the transformation $\tau = \omega_n t$. These transformations help to reduce the overall solution time. This equation is solved using HBM and TVM which are discussed in Sects. 3.4 and 3.5. The disadvantage of this method is the spread of the nonlinear function from a few physical coordinates to all the modal coordinates. Let $\mathbf{f}$ and $\mathbf{f}_{\mathrm{p}}$ are of the form $\{\mathbf{0}\ \mathbf{f}_{\mathrm{nl}}\}^T$ and $\{\mathbf{0}\ \mathbf{f}_{\mathrm{pnl}}\}^T$, but with the transformation $\mathbf{U}_L^T\mathbf{f}$ and $\mathbf{U}_L^T\mathbf{f}_{\mathrm{p}}$ it becomes $\{\mathbf{f}_{1\mathrm{nl}}\ \mathbf{f}_{2\mathrm{nl}}\}^T$ and $\{\mathbf{f}_{1\mathrm{pnl}}\ \mathbf{f}_{2\mathrm{pnl}}\}^T$. There is a natural disadvantage, since for every iteration the nonlinear force estimation alternates between modal and physical coordinates as $\mathbf{f}$ and $\mathbf{f}_{\mathrm{p}}$ are defined on the physical domain.

3.2 Dynamic substructuring

In this method, the assembled mass, stiffness, and damping matrices are partitioned into master and

Table 1 3 DOF model properties

Mass (kg)	$m_{11} = 5$	$m_{22} = 3$	$m_{33} = 1$
Damping (Ns/m)	$c_{11} = 0.15$	$c_{22} = 0.15$	$c_{33} = 0.05$
	$c_{12} = -0.10$	$c_{23} = -0.05$	
Stiffness (N/m)	$k_{11} = 6$	$k_{22} = 6$	$k_{33} = 2$
	$k_{12} = -4$	$k_{23} = -2$	
Model 1			
$f_1(x) = \alpha x_1^3$	$\alpha = 0$	$\alpha = 6$	$\alpha = 100$
$F_1(t) = F_0 + F_1 \cos \omega t$	$F_0 = 0$	$F_1 = 0.25$	$F_1 = 1.0$
Model 2			
$f_3(x) = \alpha x_3^3$	$\alpha = 0$	$\alpha = 6$	$\alpha = 100$
$F_3(t) = F_0 + F_1 \cos \omega t$	$F_0 = 0$	$F_1 = 0.25$	$F_1 = 1.0$

Table 2 Beam model properties

	Beam Axial	Beam Bending	Beam Parametric
Density (kg/m^3)	2700	2700	2700
Young's Modulus (GPa)	69	69	69
Cross section (mm × mm)	48 × 3	48 × 3	48 × 3
Length (mm)	370	370	370
DOF per node	1	2	2
Number of Elements	10	10	10
Total DOF	10	20	20
Rayleigh Damping Coeff. (Mass)	0.0245	2.45	2.45
Rayleigh Damping Coeff. (Stiffness)	1.75e–6	1.75e–3	5.25e–4
Nonlinear/Parametric Force	$k_{\text{nl}}(x) = \alpha x_1^3$	$k_{\text{nl}}(x) = \alpha x_1^3$	$F_{\text{p}} = k_{\text{p}}(1 - \alpha \cos(2\omega t))$
$F_{\text{ext}}(t) = F_0 + F_1 \cos \omega t$	$F_0 = 1.0\text{e}4$; $F_1 = 6.07\text{e}3$	$F_0 = 10.0$, $F_1 = 6.07$	$F_0 = 1.0\text{e}3$, $F_1 = 6.07$

Table 3 Details of model with internal resonance

Mass (kg)	$m_i = 20$, where $i = 1$ to 9
Stiffness (kN/m)	$k_i = 1$, where $i = 2, 3, 4, 7, 8, 10, 11, 12$
	$k_1 = k_5 = k_9 = 0.225$
Damping	Assumed Proportional
Rayleigh Damping Coeff (Mass)	0.25
Rayleigh Damping Coeff (Stiffness)	1.00e–3
$f_9(x) = \alpha x_9^3$	$\alpha = 0$; $\alpha = 1000 \times 100$; $\alpha = 1000 \times 1000$
$F_9(t) = F_0 + F_1 \cos \omega t$	$F_0 = 10$; $F_1 = 13.4$

slave subsystems. The DOF where the nonlinearity is present or where the external load is applied forms the master system and rest are considered to be slave. The mass, damping, and stiffness matrices in (1) are partitioned as shown below:

$$\mathbf{M} = \begin{bmatrix} \mathbf{M}_{\text{ss}} & \mathbf{M}_{\text{sm}} \\ \mathbf{M}_{\text{ms}} & \mathbf{M}_{\text{mm}} \end{bmatrix}; \qquad \mathbf{C} = \begin{bmatrix} \mathbf{C}_{\text{ss}} & \mathbf{C}_{\text{sm}} \\ \mathbf{C}_{\text{ms}} & \mathbf{C}_{\text{mm}} \end{bmatrix}; \qquad \mathbf{K} = \begin{bmatrix} \mathbf{K}_{\text{ss}} & \mathbf{K}_{\text{sm}} \\ \mathbf{K}_{\text{ms}} & \mathbf{K}_{\text{mm}} \end{bmatrix}. \tag{3}$$

Equation (1) can then be rewritten as

$$\begin{bmatrix} \mathbf{M}_{\text{ss}} & \mathbf{M}_{\text{sm}} \\ \mathbf{M}_{\text{ms}} & \mathbf{M}_{\text{mm}} \end{bmatrix} \begin{Bmatrix} \ddot{\mathbf{x}}_{\text{s}} \\ \ddot{\mathbf{x}}_{\text{m}} \end{Bmatrix} + \begin{bmatrix} \mathbf{C}_{\text{ss}} & \mathbf{C}_{\text{sm}} \\ \mathbf{C}_{\text{ms}} & \mathbf{C}_{\text{mm}} \end{bmatrix} \begin{Bmatrix} \dot{\mathbf{x}}_{\text{s}} \\ \dot{\mathbf{x}}_{\text{m}} \end{Bmatrix}$$

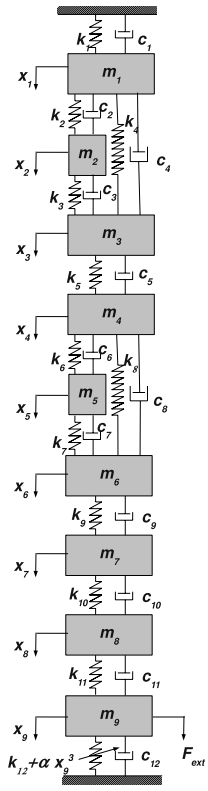

Fig. 4 System with internal resonance

(a) MDOF with internal resonance

$$+\begin{bmatrix}\mathbf{K}_{ss} & \mathbf{K}_{sm}\\ \mathbf{K}_{ms} & \mathbf{K}_{mm}\end{bmatrix}\begin{Bmatrix}\mathbf{x}_s\\ \mathbf{x}_m\end{Bmatrix}+\begin{Bmatrix}\mathbf{0}\\ \mathbf{f}_p(\mathbf{x}_m,\dot{\mathbf{x}}_m,\mathbf{t})\end{Bmatrix}$$
$$+\begin{Bmatrix}\mathbf{0}\\ \mathbf{f}(\mathbf{x}_m,\dot{\mathbf{x}}_m)\end{Bmatrix}=\begin{Bmatrix}\mathbf{0}\\ \mathbf{F}_m\end{Bmatrix}, \tag{4}$$

where $\mathbf{x}_s$ and $\mathbf{x}_m$ are the displacement DOFs associated with the slave and master partitions. The implementation details along with HBM and TVM are described in Sects. 3.4.2 and 3.5.2.

3.3 Component mode synthesis

Another approach to reduce the problem size is using component mode synthesis. The beam models analyzed are each divided into two substructures. A Craig–Bampton type substructure with more number of DOF is represented using generalized coordinates while the other substructure with nonlinearity is modeled using physical coordinates. This avoids the transformation from modal to physical coordinates for nonlinear function evaluation. Then the assembled system is partitioned into a slave and master, with the generalized coordinates forming the slave and the boundary as well as the nonlinear DOF forming the master partition.

The constraint modes of the slave substructure are defined by applying a unit displacement at each boundary freedom in turn, with all other boundary freedoms fixed and with all interior freedoms unconstrained. Equations of compatibility relate the displacements of the adjoining substructures. The final set of system generalized coordinates consists, of the system boundary generalized coordinates plus generalized coordinates for the substructure normal modes of all of the substructures. Let the governing equation of motion of the slave subsystem is given by

$$\begin{bmatrix}\mathbf{M}^1_{ii} & \mathbf{M}^1_{ij}\\ \mathbf{M}^1_{ji} & \mathbf{M}^1_{jj}\end{bmatrix}\begin{Bmatrix}\ddot{\mathbf{x}}^1_i\\ \ddot{\mathbf{x}}^1_j\end{Bmatrix}+\begin{bmatrix}\mathbf{K}^1_{ii} & \mathbf{K}^1_{ij}\\ \mathbf{K}^1_{ji} & \mathbf{K}^1_{jj}\end{bmatrix}\begin{Bmatrix}\mathbf{x}^1_i\\ \mathbf{x}^1_j\end{Bmatrix}=\mathbf{0}. \tag{5}$$

The stiffness and mass matrices of substructure 1 are partitioned into interior i and junction j DOF. Neglecting damping the normal mode of the above system is found using eigenvalue analysis. The physical coordinates of the slave system is transformed into a set of normal mode and boundary degree using the transformation

$$\begin{Bmatrix}\mathbf{x}^1_i\\ \mathbf{x}^1_j\end{Bmatrix}=\begin{bmatrix}\boldsymbol{\phi}_R & \boldsymbol{\psi}\\ \mathbf{0} & \mathbf{I}\end{bmatrix}\begin{Bmatrix}\mathbf{u}^1_i\\ \mathbf{x}^1_j\end{Bmatrix}, \tag{6}$$

where $\boldsymbol{\phi}_R$ is the matrix of retained right normal modes of interior DOF of substructure 1 (boundary DOF fixed) and $\boldsymbol{\psi}$ is the constraint mode matrix and given by

$$\boldsymbol{\psi}=-\mathbf{K}^{-1}_{ii}\mathbf{K}_{ij}. \tag{7}$$

In this paper, proportional damping is assumed. Mass, stiffness, and damping matrices are transformed into new coordinates as

$$\tilde{\mathbf{M}}^1=\begin{bmatrix}\boldsymbol{\phi}^T_L & \mathbf{0}\\ \boldsymbol{\psi}^T & \mathbf{I}\end{bmatrix}\begin{bmatrix}\mathbf{M}^1_{ii} & \mathbf{M}^1_{ij}\\ \mathbf{M}^1_{ji} & \mathbf{M}^1_{jj}\end{bmatrix}\begin{bmatrix}\boldsymbol{\phi}_R & \boldsymbol{\psi}\\ \mathbf{0} & \mathbf{I}\end{bmatrix};$$
$$\tilde{\mathbf{K}}^1=\begin{bmatrix}\boldsymbol{\phi}^T_L & \mathbf{0}\\ \boldsymbol{\psi}^T & \mathbf{I}\end{bmatrix}\begin{bmatrix}\mathbf{K}^1_{ii} & \mathbf{K}^1_{ij}\\ \mathbf{K}^1_{ji} & \mathbf{K}^1_{jj}\end{bmatrix}\begin{bmatrix}\boldsymbol{\phi}_R & \boldsymbol{\psi}\\ \mathbf{0} & \mathbf{I}\end{bmatrix}; \tag{8}$$
$$\tilde{\mathbf{C}}^1=\begin{bmatrix}\boldsymbol{\phi}^T_L & \mathbf{0}\\ \boldsymbol{\psi}^T & \mathbf{I}\end{bmatrix}\begin{bmatrix}\mathbf{C}^1_{ii} & \mathbf{C}^1_{ij}\\ \mathbf{C}^1_{ji} & \mathbf{C}^1_{jj}\end{bmatrix}\begin{bmatrix}\boldsymbol{\phi}_R & \boldsymbol{\psi}\\ \mathbf{0} & \mathbf{I}\end{bmatrix};$$

$$\tilde{\mathbf{F}}^1 = \begin{bmatrix} \boldsymbol{\phi}_L^T & \mathbf{0} \\ \boldsymbol{\psi}^T & \mathbf{I} \end{bmatrix} \begin{Bmatrix} \mathbf{F}_i^1 \\ \mathbf{F}_j^1 \end{Bmatrix}.$$

The output of this transformation $\tilde{\mathbf{K}}^1$ will lead to a diagonal matrix, where as mass $\tilde{\mathbf{M}}^1$ and the damping matrix $\tilde{\mathbf{C}}^1$ will not be diagonal. The $\{\mathbf{F}_i^1\ \mathbf{F}_j^1\}^T$ is the external force vector applied in the physical coordinate of substructure 1 and the $\tilde{\mathbf{F}}^1$ is the force vector transformed into the new coordinate system.

The governing equation of motion of the master subsystem is partitioned but no transformation is applied:

$$\begin{bmatrix} \mathbf{M}_{ii}^2 & \mathbf{M}_{ij}^2 \\ \mathbf{M}_{ji}^2 & \mathbf{M}_{jj}^2 \end{bmatrix} \begin{Bmatrix} \ddot{\mathbf{x}}_i^2 \\ \ddot{\mathbf{x}}_j^2 \end{Bmatrix} + \begin{bmatrix} \mathbf{K}_{ii}^2 & \mathbf{K}_{ij}^2 \\ \mathbf{K}_{ji}^2 & \mathbf{K}_{jj}^2 \end{bmatrix} \begin{Bmatrix} \mathbf{x}_i^2 \\ \mathbf{x}_j^2 \end{Bmatrix} = \mathbf{0}. \quad (9)$$

The stiffness and mass matrices of substructure 2 are partitioned into interior i and junction j DOF. For this subsystem the physical coordinates are kept as the same. To keep the procedure for the component mode procedure the same an identity matrix transformation is used.

$$\begin{Bmatrix} \mathbf{x}_i^2 \\ \mathbf{x}_j^2 \end{Bmatrix} = \begin{bmatrix} \mathbf{I} & \mathbf{0} \\ \mathbf{0} & \mathbf{I} \end{bmatrix} \begin{Bmatrix} \mathbf{u}_i^2 \\ \mathbf{x}_j^2 \end{Bmatrix}. \quad (10)$$

The mass, stiffness, and damping (proportional) matrices are transformed into new coordinates as

$$\begin{aligned}
\tilde{\mathbf{M}}^2 &= \begin{bmatrix} \mathbf{I} & \mathbf{0} \\ \mathbf{0} & \mathbf{I} \end{bmatrix}^T \begin{bmatrix} \mathbf{M}_{ii}^1 & \mathbf{M}_{ij}^1 \\ \mathbf{M}_{ji}^1 & \mathbf{M}_{jj}^1 \end{bmatrix} \begin{bmatrix} \mathbf{I} & \mathbf{0} \\ \mathbf{0} & \mathbf{I} \end{bmatrix}, \\
\tilde{\mathbf{K}}^2 &= \begin{bmatrix} \mathbf{I} & \mathbf{0} \\ \mathbf{0} & \mathbf{I} \end{bmatrix}^T \begin{bmatrix} \mathbf{K}_{ii}^1 & \mathbf{K}_{ij}^1 \\ \mathbf{K}_{ji}^1 & \mathbf{K}_{jj}^1 \end{bmatrix} \begin{bmatrix} \mathbf{I} & \mathbf{0} \\ \mathbf{0} & \mathbf{I} \end{bmatrix}, \\
\tilde{\mathbf{C}}^2 &= \begin{bmatrix} \mathbf{I} & \mathbf{0} \\ \mathbf{0} & \mathbf{I} \end{bmatrix}^T \begin{bmatrix} \mathbf{C}_{ii}^1 & \mathbf{C}_{ij}^1 \\ \mathbf{C}_{ji}^1 & \mathbf{C}_{jj}^1 \end{bmatrix} \begin{bmatrix} \mathbf{I} & \mathbf{0} \\ \mathbf{0} & \mathbf{I} \end{bmatrix}, \\
\tilde{\mathbf{f}}_{\mathrm{p}}^2 &= \begin{bmatrix} \mathbf{I} & \mathbf{0} \\ \mathbf{0} & \mathbf{I} \end{bmatrix}^T \begin{Bmatrix} \mathbf{f}_{\mathrm{p}i}^2 \\ \mathbf{f}_{\mathrm{p}j}^2 \end{Bmatrix}, \\
\tilde{\mathbf{f}}^2 &= \begin{bmatrix} \mathbf{I} & \mathbf{0} \\ \mathbf{0} & \mathbf{I} \end{bmatrix}^T \begin{Bmatrix} \mathbf{f}_i^2 \\ \mathbf{f}_j^2 \end{Bmatrix}, \\
\tilde{\mathbf{F}}^2 &= \begin{bmatrix} \mathbf{I} & \mathbf{0} \\ \mathbf{0} & \mathbf{I} \end{bmatrix}^T \begin{Bmatrix} \mathbf{F}_i^2 \\ \mathbf{F}_j^2 \end{Bmatrix},
\end{aligned} \quad (11)$$

$\{\mathbf{f}_i^2\ \mathbf{f}_j^2\}^T$ is the nonlinear function at the physical coordinate and $\tilde{\mathbf{f}}^2$ is the nonlinear function transformed into the new coordinate system. $\{\mathbf{F}_i^2\ \mathbf{F}_j^2\}^T$ is the external force vector applied in the physical coordinate of substructure 2 and $\tilde{\mathbf{F}}^2$ is the force vector transformed into the new coordinate system. The subsystem 1 and subsystem 2 have a common interface. Physical displacements at the interface are constrained by

$$\mathbf{x}_j^1 = \mathbf{x}_j^2. \quad (12)$$

The assembled coordinate transformation matrix is given by

$$\mathbf{u} = \begin{Bmatrix} \mathbf{u}_i^1 \\ \mathbf{x}_j^1 \\ \mathbf{u}_i^2 \end{Bmatrix} = \begin{bmatrix} \mathbf{I} & \mathbf{0} & \mathbf{0} & \mathbf{0} \\ \mathbf{0} & \mathbf{I} & \mathbf{0} & \mathbf{I} \\ \mathbf{0} & \mathbf{0} & \mathbf{I} & \mathbf{0} \end{bmatrix} \begin{Bmatrix} \mathbf{u}_i^1 \\ \mathbf{x}_j^1 \\ \mathbf{u}_i^2 \\ \mathbf{x}_j^2 \end{Bmatrix} = \mathbf{S} \begin{Bmatrix} \mathbf{u}_i^1 \\ \mathbf{x}_j^1 \\ \mathbf{u}_i^2 \\ \mathbf{x}_j^2 \end{Bmatrix}. \quad (13)$$

The transformed nonlinear function as well as the external and parametric excitation forces are

$$\begin{aligned}
\mathbf{f} &= \begin{Bmatrix} \mathbf{f}_i^1 \\ \mathbf{f}_j^1 \\ \mathbf{f}_i^2 \end{Bmatrix} = \mathbf{S} \begin{Bmatrix} \mathbf{0} \\ \mathbf{0} \\ \mathbf{f}_i^2 \\ \mathbf{f}_j^2 \end{Bmatrix}; \\
\mathbf{f}_{\mathrm{p}} &= \begin{Bmatrix} \mathbf{f}_{\mathrm{p}i}^1 \\ \mathbf{f}_{\mathrm{p}j}^1 \\ \mathbf{f}_{\mathrm{p}i}^2 \end{Bmatrix} = \mathbf{S} \begin{Bmatrix} \mathbf{0} \\ \mathbf{0} \\ \mathbf{f}_{\mathrm{p}i}^2 \\ \mathbf{f}_{\mathrm{p}j}^2 \end{Bmatrix}; \\
\mathbf{F} &= \begin{Bmatrix} \mathbf{F}_i^1 \\ \mathbf{F}_j^1 \\ \mathbf{F}_i^2 \end{Bmatrix} = \mathbf{S} \begin{Bmatrix} \mathbf{F}_i^1 \\ \mathbf{F}_j^1 \\ \mathbf{F}_i^2 \\ \mathbf{F}_j^2. \end{Bmatrix}.
\end{aligned} \quad (14)$$

The assembled mass, damping stiffness, and the force matrices are

$$\begin{aligned}
\tilde{\mathbf{M}} &= \begin{bmatrix} \tilde{\mathbf{M}}_{ii}^1 & \mathbf{0} & \mathbf{0} & \mathbf{0} \\ \mathbf{0} & \tilde{\mathbf{M}}_{jj}^1 & \mathbf{0} & \mathbf{0} \\ \mathbf{0} & \mathbf{0} & \tilde{\mathbf{M}}_{ii}^2 & \mathbf{0} \\ \mathbf{0} & \mathbf{0} & \mathbf{0} & \tilde{\mathbf{M}}_{jj}^2 \end{bmatrix}; \\
\tilde{\mathbf{C}} &= \begin{bmatrix} \tilde{\mathbf{C}}_{ii}^1 & \mathbf{0} & \mathbf{0} & \mathbf{0} \\ \mathbf{0} & \tilde{\mathbf{C}}_{jj}^1 & \mathbf{0} & \mathbf{0} \\ \mathbf{0} & \mathbf{0} & \tilde{\mathbf{C}}_{ii}^2 & \mathbf{0} \\ \mathbf{0} & \mathbf{0} & \mathbf{0} & \tilde{\mathbf{C}}_{jj}^2 \end{bmatrix};
\end{aligned} \quad (15)$$

$$\tilde{\mathbf{K}} = \begin{bmatrix} \tilde{\mathbf{K}}^1_{ii} & \mathbf{0} & \mathbf{0} & \mathbf{0} \\ \mathbf{0} & \tilde{\mathbf{K}}^1_{jj} & \mathbf{0} & \mathbf{0} \\ \mathbf{0} & \mathbf{0} & \tilde{\mathbf{K}}^2_{ii} & \mathbf{0} \\ \mathbf{0} & \mathbf{0} & \mathbf{0} & \tilde{\mathbf{K}}^2_{jj} \end{bmatrix}.$$

The combined mass, damping, and stiffness of the substructures are

$$\mathbf{M} = \mathbf{S}^T \tilde{\mathbf{M}} \mathbf{S}; \qquad \mathbf{C} = \mathbf{S}^T \tilde{\mathbf{C}} \mathbf{S}; \quad \mathbf{K} = \mathbf{S}^T \tilde{\mathbf{K}} \mathbf{S}. \tag{16}$$

Combining (14) and (16), the final equation for the full model is

$$\mathbf{M}\ddot{\mathbf{u}} + \mathbf{C}\dot{\mathbf{u}} + \mathbf{K}\mathbf{u} + \mathbf{f}_{\mathrm{p}} + \mathbf{f} = \mathbf{F}. \tag{17}$$

The structure of the matrices **M**, **C**, and **K** will be as follows and they are of size $(nmode + nj + nn) \times (nmode + nj + nn)$. Where *nmode* is the number of included modes of substructure 1, *nj* is the number of boundary DOF, and *nn* is the number of DOF of the substructure 2 (which contains the nonlinear DOF).

$$\mathbf{M} = \begin{bmatrix} \mathbf{M}_{\mathrm{ss}} & \mathbf{M}_{\mathrm{sm}} \\ \mathbf{M}_{\mathrm{ms}} & \mathbf{M}_{\mathrm{mm}} \end{bmatrix};$$

$$\mathbf{C} = \begin{bmatrix} \mathbf{C}_{\mathrm{ss}} & \mathbf{C}_{\mathrm{sm}} \\ \mathbf{C}_{\mathrm{ms}} & \mathbf{C}_{\mathrm{mm}} \end{bmatrix}; \tag{18}$$

$$\mathbf{K} = \begin{bmatrix} \mathbf{K}_{\mathrm{ss}} & \mathbf{0} \\ \mathbf{0} & \mathbf{K}_{\mathrm{mm}} \end{bmatrix}.$$

The assembled stiffness matrix is diagonal because the static Green's function solution which is used as a constraint mode, diagonalizes the stiffness matrix, but leads to an inertia coupling which is evident in the mass matrix structure. So (17) can be rewritten as

$$\begin{bmatrix} \mathbf{M}_{\mathrm{ss}} & \mathbf{M}_{\mathrm{sm}} \\ \mathbf{M}_{\mathrm{ms}} & \mathbf{M}_{\mathrm{mm}} \end{bmatrix} \begin{Bmatrix} \ddot{\mathbf{u}}_{\mathrm{s}} \\ \ddot{\mathbf{u}}_{\mathrm{m}} \end{Bmatrix} + \begin{bmatrix} \mathbf{C}_{\mathrm{ss}} & \mathbf{C}_{\mathrm{sm}} \\ \mathbf{C}_{\mathrm{ms}} & \mathbf{C}_{\mathrm{mm}} \end{bmatrix} \begin{Bmatrix} \dot{\mathbf{u}}_{\mathrm{s}} \\ \dot{\mathbf{u}}_{\mathrm{m}} \end{Bmatrix} + \begin{bmatrix} \mathbf{K}_{\mathrm{ss}} & \mathbf{0} \\ \mathbf{0} & \mathbf{K}_{\mathrm{mm}} \end{bmatrix} \begin{Bmatrix} \mathbf{u}_{\mathrm{s}} \\ \mathbf{u}_{\mathrm{m}} \end{Bmatrix} + \begin{Bmatrix} \mathbf{0} \\ \mathbf{f}_{\mathrm{p}} \end{Bmatrix} + \begin{Bmatrix} \mathbf{0} \\ \mathbf{f} \end{Bmatrix} = \begin{Bmatrix} \mathbf{F}_{\mathrm{s}} \\ \mathbf{F}_{\mathrm{m}} \end{Bmatrix}. \tag{19}$$

where $\mathbf{u}_{\mathrm{s}}$ and $\mathbf{u}_{\mathrm{m}}$ are the slave and master displacement DOF. Slave DOF consists of only the included modes of substructure 1 and the master DOF consists of the boundary DOF and the physical DOF of substructure 2.

Systems with internal resonances have eigenvalues (natural frequencies) which are integer multiples of one or more eigenvalues. Only when a 1:1 internal resonance occurs, generalized eigenvectors need to be generated for forming the complete independent basis vectors. However, defective symmetric systems are guaranteed to have orthogonal eigenvectors [29]. There are three possible scenarios with the modeling strategy proposed. For the first case, the entire system has a 1:1 internal resonance, but the slave system after partitioning does not have an internal resonance. The second scenario is where the slave system also has a 1:1 internal resonance, and finally the case where the full system has no internal resonance but the slave partition has an internal resonance. Since the first scenario can be handled by the procedure outlined earlier, only the second and third scenarios need to be examined. One MDOF case is taken as an example case (Fig. 4), where the slave system as well as the full system have a nearly 1:1 internal resonance.

3.4 Harmonic balance method

In HBM, the kth element of the response vector, external force vector and the nonlinear function are expressed as a truncated Fourier series of n terms as shown below

$$x_k(t) = \tilde{x}_{k0} + \sum_{l=1}^{n} \left\{ \tilde{x}^c_{kl} \cos(l\omega t) + \tilde{x}^s_{kl} \sin(l\omega t) \right\}, \tag{20}$$

$$F_k(t) = \tilde{F}_{k0} + \sum_{l=1}^{n} \left\{ \tilde{F}^c_{kl} \cos(l\omega t) + \tilde{F}^s_{kl} \sin(l\omega t) \right\}, \tag{21}$$

$$f_k(x, \dot{x}) = \tilde{f}_{k0} + \sum_{l=1}^{n} \left\{ \tilde{f}^c_{kl} \cos(l\omega t) + \tilde{f}^s_{kl} \sin(l\omega t) \right\}, \tag{22}$$

$$f_{\mathrm{p}k}(x, \dot{x}) = \tilde{f}_{\mathrm{p}k0} + \sum_{l=1}^{n} \left\{ \tilde{f}^c_{\mathrm{p}kl} \cos(l\omega t) + \tilde{f}^s_{\mathrm{p}kl} \sin(l\omega t) \right\}, \tag{23}$$

where $k = 1, 2, 3, \ldots, N$ with N being the number of DOF. Substituting these into (1) leads to

$$\begin{bmatrix} \mathbf{E}_{11} & \mathbf{E}_{12} & \cdots & \mathbf{E}_{1N} \\ \mathbf{E}_{21} & \mathbf{E}_{22} & \cdots & \mathbf{E}_{2N} \\ \vdots & \vdots & \ddots & \vdots \\ \mathbf{E}_{N1} & \mathbf{E}_{N2} & \cdots & \mathbf{E}_{NN} \end{bmatrix} \begin{Bmatrix} \tilde{\mathbf{x}}_1 \\ \tilde{\mathbf{x}}_2 \\ \vdots \\ \tilde{\mathbf{x}}_N \end{Bmatrix} + \begin{Bmatrix} \tilde{\mathbf{f}}_{\mathrm{p}_1} \\ \tilde{\mathbf{f}}_{\mathrm{p}_2} \\ \vdots \\ \tilde{\mathbf{f}}_{\mathrm{p}_N} \end{Bmatrix} + \begin{Bmatrix} \tilde{\mathbf{f}}_1 \\ \tilde{\mathbf{f}}_2 \\ \vdots \\ \tilde{\mathbf{f}}_N \end{Bmatrix} - \begin{Bmatrix} \tilde{\mathbf{F}}_1 \\ \tilde{\mathbf{F}}_2 \\ \vdots \\ \tilde{\mathbf{F}}_N \end{Bmatrix} = \mathbf{R}(\alpha), \tag{24}$$

where $\mathbf{R}(\gamma)$ is the residual error in the Fourier series truncation (as Fourier series is an infinite series) and $\tilde{\mathbf{x}}_{..}, \tilde{\mathbf{f}}_{..}, \tilde{\mathbf{F}}_{..}$ represents the vector containing the Fourier coefficients arranged as constant term, cosine term, and sine term in sequence for a particular DOF. For example, $\tilde{\mathbf{x}}_i$ is given by $\{\tilde{x}_{i0}, \tilde{x}^c_{i1}, \tilde{x}^s_{i1}, \tilde{x}^c_{i2}, \tilde{x}^s_{i2}, \ldots, \tilde{x}^c_{in}, \tilde{x}^s_{in}\}^T$. $\mathbf{E}_{ij}$ will have the following structure and is of size $(2n+1) \times (2n+1)$.

$$\mathbf{E}_{ij} = \begin{bmatrix} k_{ij} & 0 & 0 & \cdots & 0 & 0 \\ 0 & k_{ij} - \omega^2 m_{ij} & \omega c_{ij} & \cdots & 0 & 0 \\ 0 & -\omega c_{ij} & k_{ij} - \omega^2 m_{ij} & \cdots & 0 & 0 \\ \vdots & \vdots & \vdots & \ddots & \vdots & \vdots \\ 0 & 0 & 0 & \cdots & k_{ij} - n^2\omega^2 m_{ij} & n\omega c_{ij} \\ 0 & 0 & 0 & \cdots & -n\omega c_{ij} & k_{ij} - n^2\omega^2 m_{ij} \end{bmatrix}. \tag{25}$$

This residual is minimized as

$$\sum_{n=1}^{m} \left[\int_0^{2\pi/\omega} R(\alpha) \begin{pmatrix} 1 \\ \cos(n\omega t) \\ \sin(n\omega t) \end{pmatrix} dt \right] = 0 \tag{26}$$

leading to

$$\mathbf{Y}\tilde{\mathbf{x}}_{\mathrm{a}} + +\tilde{\mathbf{f}}_{\mathrm{p}} + \tilde{\mathbf{f}} - \tilde{\mathbf{F}} = \mathbf{0}. \tag{27}$$

The above algebraic equation is solved using Newton–Raphson procedure. The initial value for $\tilde{x}_{\mathrm{a}}$ is calculated from the linear equation and this value is used for computing $\{x\}$ and $\{\dot{x}\}$ at discrete time points (say js), over $t \in [0, 2\pi/\omega]$ for a time step of $\Delta t = 2\pi/(js.\omega)$. Care should be taken while selecting the sample size to avoid aliasing. From these displacement and velocity values, a Discrete Fourier Transform (DFT) is performed to get the nonlinear function Fourier coefficients. The Newton–Raphson procedure requires the calculation of the Jacobian for every iteration. The Jacobian is given by

$$\mathbf{J} = \frac{\partial(\mathbf{Y}\tilde{\mathbf{x}}_{\mathrm{a}} + \tilde{\mathbf{f}}_{\mathrm{p}} + \tilde{\mathbf{f}} - \tilde{\mathbf{F}})}{\partial \tilde{\mathbf{x}}_{\mathrm{a}}}. \tag{28}$$

The iteration is said to have converged when $\|\Delta\tilde{\mathbf{x}}^i_{\mathrm{a}}\| < \epsilon$ where i is the iteration number, ϵ is the prescribed convergence tolerance. The L_∞ norm is used for checking convergence and the L_2 norm of the residue is also checked to assure complete convergence.

3.4.1 Mode superposition with HBM

Here, mass, damping, and stiffness matrix are taken from the reduced system given by (2). The rest of the procedure is same as above. But in case of HBM, the size of the problem will be increased by the number of harmonics included in Fourier series. For example, let the number of harmonics included in the Fourier series be $nhar$. Then the total size of the problem for a N DOF system will be increased to $(N \times 2nhar + 1) \times (N \times 2nhar + 1)$ from its original size of $N \times N$. This is better than numerical integration, as in general the Newton–Raphson will converge in fewer iterations.

3.4.2 Dynamic substructuring with HBM

The final nonlinear algebraic equation is given below. Let $\tilde{\mathbf{x}}_{\mathrm{s}}$ represents the coefficients from HBM for the slave DOF and $\tilde{\mathbf{x}}_{\mathrm{m}}$ represents the coefficients from

HBM for master DOF and $\tilde{\mathbf{f}}$ and $\tilde{\mathbf{F}}$ are the coefficients from HBM for nonlinear and external force terms.

$$\begin{bmatrix} \mathbf{Y}_{ss} & \mathbf{Y}_{sm} \\ \mathbf{Y}_{ms} & \mathbf{Y}_{mm} \end{bmatrix} \begin{Bmatrix} \tilde{\mathbf{x}}_s \\ \tilde{\mathbf{x}}_m \end{Bmatrix} + \begin{Bmatrix} \mathbf{0} \\ \tilde{\mathbf{f}}_p \end{Bmatrix} + \begin{Bmatrix} \mathbf{0} \\ \tilde{\mathbf{f}} \end{Bmatrix} = \begin{Bmatrix} \mathbf{0} \\ \tilde{\mathbf{F}} \end{Bmatrix}, \quad (29)$$

which leads to

$$\tilde{\mathbf{x}}_s = -\mathbf{Y}_{ss}^{-1}(\mathbf{Y}_{sm}\tilde{\mathbf{x}}_m). \quad (30)$$

Substituting this into the equation of $\tilde{\mathbf{x}}_m$ gives

$$\left(\mathbf{Y}_{mm} - \mathbf{Y}_{ms}\mathbf{Y}_{ss}^{-1}\mathbf{Y}_{sm}\right)\tilde{\mathbf{x}}_m + \tilde{\mathbf{f}}_p + \tilde{\mathbf{f}} = \tilde{\mathbf{F}}. \quad (31)$$

If only stiffness matrix is considered for condensation, then it is known as a static condensation, while in the present paper dynamic condensation is carried out, which includes both mass as well as damping. In the present methods, while forming $\mathbf{Y}_{ss}$ and $\mathbf{Y}_{sm}$, damping is also included. This equation is smaller in size compared to the original structure as it contains only the nonlinear DOF (which will be less in number) and external force DOF which also will be less in number. The negative side of this method is that it requires inversion of the frequency dependent slave flexibility matrix (size of which will be comparable) for every iteration.

3.4.3 *Component mode synthesis based dynamic substructuring with HBM*

Equation (19) represents the final assembled form of the reduced system using CMS. Let $\tilde{\mathbf{u}}_{sf}$ represent the Fourier coefficient displacement vector for slave DOF and $\tilde{\mathbf{u}}_{mf}$ are Fourier coefficient displacement vector for master DOF. The Fourier coefficient vectors $\tilde{\mathbf{f}}$, $\tilde{\mathbf{F}}_s$, and $\tilde{\mathbf{F}}_m$ represent the nonlinear function and external excitation terms of the slave and the master DOF, respectively. Equation (27) can be written in the form

$$\begin{bmatrix} \mathbf{Y}_{ss} & \mathbf{Y}_{sm} \\ \mathbf{Y}_{ms} & \mathbf{Y}_{mm} \end{bmatrix} \begin{Bmatrix} \tilde{\mathbf{u}}_{sf} \\ \tilde{\mathbf{u}}_{mf} \end{Bmatrix} + \begin{Bmatrix} \mathbf{0} \\ \tilde{\mathbf{f}}_p \end{Bmatrix} + \begin{Bmatrix} \mathbf{0} \\ \tilde{\mathbf{f}} \end{Bmatrix} = \begin{Bmatrix} \tilde{\mathbf{F}}_s \\ \tilde{\mathbf{F}}_m \end{Bmatrix}, \quad (32)$$

which leads to

$$\tilde{\mathbf{u}}_{sf} = -\mathbf{Y}_{ss}^{-1}\left(\tilde{\mathbf{F}}_s - \mathbf{Y}_{sm}\tilde{\mathbf{u}}_{mf}\right). \quad (33)$$

Substituting this into the equation of $\tilde{\mathbf{x}}_{mf}$ gives

$$\left(\mathbf{Y}_{mm} - \mathbf{Y}_{ms}\mathbf{Y}_{ss}^{-1}\mathbf{Y}_{sm}\right)\tilde{\mathbf{u}}_{mf} + \tilde{\mathbf{f}}_p + \tilde{\mathbf{f}} = \tilde{\mathbf{F}}_m - \mathbf{Y}_{ms}Y_{ss}^{-1}\tilde{\mathbf{F}}_s. \quad (34)$$

This equation will be of very small size compared to the original structure as it contains only the nonlinear substructure DOF (which will be less in number) and the boundary DOF which also will be less in number. The only disadvantage of this method is that it requires inversion of the frequency dependent slave flexibility matrix for every iteration. But this disadvantage is avoided in this paper by the arrangement of Fourier coefficients as shown in Sect. 3.4. From component mode synthesized matrix, the mass matrix $\mathbf{M}_{ss}$ and $\mathbf{K}_{ss}$ will be diagonal, and Fourier coefficients arrangement as above gives a structure for $\mathbf{Y}_{ss}$ as $\mathbf{Y}_{ss} = [\text{diag}\{\mathbf{H}_1, \mathbf{H}_2, \ldots, \mathbf{H}_l\}]$, where l is the number of kept modes of the substructure 1 and n is the number of harmonics.

$$\mathbf{H}_i = \begin{bmatrix} \Omega_{si}^2 & 0 & 0 & 0 & 0 & \ldots & 0 & 0 \\ 0 & \Omega_{si}^2 - \omega^2 & 2\zeta\omega\Omega_{si} & 0 & 0 & \ldots & 0 & 0 \\ 0 & -2\zeta\omega\Omega_{si} & \Omega_{si}^2 - \omega^2 & 0 & 0 & \ldots & 0 & 0 \\ 0 & 0 & 0 & \Omega_{si}^2 - 4\omega^2 & 4\zeta\omega\Omega_{si} & \ldots & 0 & 0 \\ 0 & 0 & 0 & -4\zeta\omega\Omega_{si} & \Omega_{si}^2 - 4\omega^2 & \ldots & 0 & 0 \\ \vdots & \vdots & \vdots & \vdots & \vdots & \ddots & \vdots & \vdots \\ 0 & 0 & 0 & 0 & 0 & \ldots & \Omega_{si}^2 - n^2\omega^2 & 2n\zeta\omega\Omega_{si} \\ 0 & 0 & 0 & 0 & 0 & \ldots & -2n\zeta\omega\Omega_{si} & \Omega_{si}^2 - n^2\omega^2 \end{bmatrix}, \quad (35)$$

which is block diagonal and whose inverse can be evaluated analytically, hence avoiding the inverse calculation for each iteration; where Ω_{si}th is the natural frequency for ith natural mode of the substructure 1. The only cost involved is in the evaluation of this matrix in addition to the evaluation of $\mathbf{Y}_{ss}$. The inverse of the $\mathbf{Y}_{ss}$ is given as $\mathbf{Y}_{ss}^{-1} = [\text{diag}\{\mathbf{B}_1, \mathbf{B}_2, \ldots, \mathbf{B}_l\}]$, where l is the number of kept modes of the substructure 1

$$\mathbf{B}_i^{-1} = \begin{bmatrix} 1/\Omega_{si}^2 & 0 & 0 & 0 & 0 & \ldots & 0 & 0 \\ 0 & B_i^{11} & -B_i^{12} & 0 & 0 & \ldots & 0 & 0 \\ 0 & B_i^{12} & B_i^{12} & 0 & 0 & \ldots & 0 & 0 \\ 0 & 0 & 0 & B_i^{21} & -B_i^{22} & \ldots & 0 & 0 \\ 0 & 0 & 0 & B_i^{22} & B_i^{21} & \ldots & 0 & 0 \\ \vdots & \vdots & \vdots & \vdots & \vdots & \ddots & \vdots & \vdots \\ 0 & 0 & 0 & 0 & 0 & \ldots & B_i^{n1} & -B_i^{n2} \\ 0 & 0 & 0 & 0 & 0 & \ldots & B_i^{n2} & B_i^{n1} \end{bmatrix}, \tag{36}$$

where Ω_{si} is the ith natural frequency and n is the number of harmonics.

$$\begin{aligned} B_i^{j1} &= \frac{\Omega_{si}^2 - j^2\omega^2}{(\Omega_{si}^2 - j^2\omega^2)^2 + (2j\zeta\omega\Omega_{si})^2}; \\ B_i^{j2} &= \frac{2j\zeta\omega\Omega_{si}}{(\Omega_{si}^2 - j^2\omega^2)^2 + (2j\zeta\omega\Omega_{si})^2}. \end{aligned} \tag{37}$$

The differential matrices for the continuation algorithm also changes. They are calculated appropriately, and given in Appendix B.1 Hence, the nonlinear problem can be solved accurately using less number of DOF without losing accuracy and without explicitly calculating the inverse for each iteration. It also avoids the inverse update using the Sherman–Morrison approximation [29].

3.5 Time variational formulation (TVM)

The governing equations of motion given by (1) in physical time is transformed to a nondimensional time using $\tau = \omega t$, where ω is the excitation frequency. Applying the above time scaling into (1) leads to

$$\omega^2\mathbf{M}\mathbf{x}'' + \omega\mathbf{C}\mathbf{x}' + \mathbf{K}\mathbf{x} + \mathbf{f}_{\text{p}}(\mathbf{x}, \mathbf{x}', \tau) + \mathbf{f}(\mathbf{x}, \mathbf{x}') = \mathbf{F}(\tau), \tag{38}$$

where $\mathbf{x}'$ and $\mathbf{x}''$ are the first and second derivatives of x with respect to τ. Displacement, velocity, acceleration, nonlinear function, and external force are expressed in terms of the approximated basis functions say $\Phi(\tau)$. Unlike the HBM, where trigonometric functions used have global support, these basis functions will have only local support (like finite element shape functions). Details of the type of basis functions and its properties and structure of the differentiation matrix can be obtained from the paper by Rook [23]. In this paper, the hat function is used as a basis function. As in harmonic balance, these variables are substituted back into (38) and the resulting weak form residual is formed as given below.

$$\begin{aligned} \mathbf{R}(\hat{\mathbf{x}}) = &\left[\omega^2\left(\mathbf{M} \otimes \mathbf{D}^{(2)}\right) + \omega\left(\mathbf{C} \otimes \mathbf{D}^{(1)}\right) + \left(\mathbf{K} \otimes \mathbf{D}^{(0)}\right)\right] \\ &\times \{\hat{\mathbf{x}}\} + \hat{\mathbf{f}}_{\text{p}}(\hat{\mathbf{x}}) + \hat{\mathbf{f}}(\hat{\mathbf{x}}) - \hat{\mathbf{F}}, \end{aligned} \tag{39}$$

where $\otimes$ is the Kronecker product; $\mathbf{D}^{(2)}$, $\mathbf{D}^{(1)}$ are the second and first derivative matrix of the basis function matrix $\mathbf{D}^{(0)}$. The nonlinear and external force values evaluated at the discrete time points are given by $\hat{\mathbf{f}}(\hat{\mathbf{x}})$ and $\hat{\mathbf{F}}$. Equation (38) can then be rewritten as

$$\mathbf{Y}\hat{\mathbf{x}} + \hat{\mathbf{f}}_{\text{p}}(\hat{\mathbf{x}}) + \hat{\mathbf{f}}(\hat{\mathbf{x}}) - \hat{\mathbf{F}} = 0. \tag{40}$$

This leads to a set of nonlinear algebraic equation, which can be solved using Newton–Raphson procedure with the Jacobian calculated as

$$\mathbf{J} = \frac{\partial}{\partial\tilde{\mathbf{x}}}\left\{\mathbf{Y}\tilde{\mathbf{x}} + \tilde{\mathbf{f}}_{\text{p}} + \tilde{\mathbf{f}} - \tilde{\mathbf{F}}\right\}. \tag{41}$$

The iteration is said to have converged when $\|\Delta\tilde{\mathbf{x}}^i\| < \epsilon$ where i is the iteration number, ϵ is the prescribed convergence tolerance. The main advantage of this method is the sparse structure of the resulting Jacobian due to the local support of basis vectors. Hence, the solution can be carried out very fast using sparse solvers.

3.5.1 Mode superposition with TVM

Here, mass, damping, and stiffness matrix are taken from the reduced system given by (2). The rest of the procedure is same as above. In case of time variational formulation with Np time points, total size of the problem for a N DOF system will be increased to $(N \times Np) \times (N \times Np)$ from its original size of $(N \times N)$.

3.5.2 Dynamic substructuring with TVM

The final nonlinear algebraic equation is given below. Let $\tilde{\mathbf{x}}_{\text{s}}$ represents the coefficients from TVM for slave

DOF and $\tilde{\mathbf{x}}_{\mathrm{m}}$ represents the coefficients from TVM for master DOF and $\tilde{\mathbf{f}}$ and $\tilde{\mathbf{F}}$ are coefficients from TVM for nonlinear and external force terms.

$$\begin{bmatrix} \mathbf{Y}_{\mathrm{ss}} & \mathbf{Y}_{\mathrm{sm}} \\ \mathbf{Y}_{\mathrm{ms}} & \mathbf{Y}_{\mathrm{mm}} \end{bmatrix} \begin{Bmatrix} \tilde{\mathbf{x}}_{\mathrm{s}} \\ \tilde{\mathbf{x}}_{\mathrm{m}} \end{Bmatrix} + \begin{Bmatrix} \mathbf{0} \\ \tilde{\mathbf{f}}_{\mathrm{p}} \end{Bmatrix} + \begin{Bmatrix} \mathbf{0} \\ \tilde{\mathbf{f}} \end{Bmatrix} = \begin{Bmatrix} \mathbf{0} \\ \tilde{\mathbf{F}} \end{Bmatrix}, \quad (42)$$

which leads to

$$\tilde{\mathbf{x}}_{\mathrm{s}} = -\mathbf{Y}_{\mathrm{ss}}^{-1}(Y_{\mathrm{sm}}\tilde{\mathbf{x}}_{\mathrm{m}}). \quad (43)$$

Substituting this into the equation of $\tilde{\mathbf{x}}_{\mathrm{m}}$ gives

$$\left(\mathbf{Y}_{\mathrm{mm}} - \mathbf{Y}_{\mathrm{ms}}\mathbf{Y}_{\mathrm{ss}}^{-1}\mathbf{Y}_{\mathrm{sm}}\right)\tilde{\mathbf{x}}_{\mathrm{m}} + \tilde{\mathbf{f}}_{\mathrm{p}} + \tilde{\mathbf{f}} = \tilde{\mathbf{F}}. \quad (44)$$

In the present methods while forming $\mathbf{Y}_{\mathrm{ss}}$ and $\mathbf{Y}_{\mathrm{sm}}$, damping is also included. This equation is smaller in size compared to the original structure as it contains only the nonlinear DOF (which will be less in number) and the external force DOF which are also small in number. The downside of this method is that it requires the inverse of the frequency dependent slave flexibility matrix ($\mathbf{Y}_{\mathrm{ss}}$) for every iteration (size of which will be comparable to the full system). In addition, the $\mathbf{Y}_{\mathrm{ss}}$ is also discretized in time.

3.5.3 Component mode synthesis based dynamic substructuring with TVM

Equation (19) represents the final assembled form of the reduced system. Let $\tilde{\mathbf{u}}_{\mathrm{s}f}$ represents TVM coefficients for slave DOF and $\tilde{\mathbf{u}}_{\mathrm{m}f}$ are coefficients for master DOF and $\tilde{\mathbf{f}}$, $\tilde{\mathbf{F}}_{,\mathrm{s}}$ and $\tilde{\mathbf{F}}_{\mathrm{s}}$ are coefficients of the nonlinear function and coefficients of the slave and the master DOF external force, respectively. Equation (40) can be written in the form

$$\begin{bmatrix} \mathbf{Y}_{\mathrm{ss}} & \mathbf{Y}_{\mathrm{sm}} \\ \mathbf{Y}_{\mathrm{ms}} & \mathbf{Y}_{\mathrm{mm}} \end{bmatrix} \begin{Bmatrix} \tilde{\mathbf{u}}_{\mathrm{s}f} \\ \tilde{\mathbf{u}}_{\mathrm{m}f} \end{Bmatrix} + \begin{Bmatrix} \mathbf{0} \\ \tilde{\mathbf{f}}_{\mathrm{p}} \end{Bmatrix} + \begin{Bmatrix} \mathbf{0} \\ \tilde{\mathbf{f}} \end{Bmatrix} = \begin{Bmatrix} \tilde{\mathbf{F}}_{\mathrm{s}} \\ \tilde{\mathbf{F}}_{\mathrm{m}} \end{Bmatrix}, \quad (45)$$

which leads to

$$\tilde{\mathbf{u}}_{\mathrm{s}f} = -\mathbf{Y}_{\mathrm{ss}}^{-1}\left(\tilde{\mathbf{F}}_{\mathrm{s}} - \mathbf{Y}_{\mathrm{sm}}\tilde{\mathbf{u}}_{\mathrm{m}f}\right). \quad (46)$$

Substituting this into the equation of $\tilde{\mathbf{x}_{\mathrm{m}f}}$ gives

$$\left(\mathbf{Y}_{\mathrm{mm}} - Y_{\mathrm{ms}}\mathbf{Y}_{\mathrm{ss}}^{-1}\mathbf{Y}_{\mathrm{sm}}\right)\tilde{\mathbf{u}}_{\mathrm{m}f} + \tilde{\mathbf{f}}_{\mathrm{p}} + \tilde{\mathbf{f}} = \tilde{\mathbf{F}}_{\mathrm{m}} - \mathbf{Y}_{\mathrm{ms}}\mathbf{Y}_{\mathrm{ss}}^{-1}\tilde{\mathbf{F}}_{\mathrm{s}}. \quad (47)$$

This equation will be of very small size compared to the original structure as it contains only the nonlinear substructure DOF (which will be less in number) and the boundary DOF which also will be less in number. The disadvantage of this method is that it requires the frequency dependent slave flexibility matrix for every iteration (involves an inverse calculation). As in the case of dynamic substructuring, slave dynamic flexibility matrix for every frequency iteration (involves an inverse calculation), but the advantage is that the slave dynamic flexibility matrix has a sparse structure.

3.6 Parametric continuation

As the solution of the above nonlinear problem contains many solution branches for the given set of conditions, it is important to trace all of them. Hence, for a given amplitude of external force or for a particular frequency of excitation, multiple solutions are possible which depends on whether the solution is in the forward sweep or in the backward sweep. Regular numerical integration procedures will not give the entire solution due to the fact that it will converge only to the stable solution. Hence, in order to trace the entire solution space, a continuation method is necessary. The most commonly used continuation method is the Homotopy method, where the N nonlinear equations in N nonlinear variables $\mathbf{f}(\mathbf{x}) = \mathbf{0}$ are converted into a new system of equations by adding another variable $x_{N+1} = \lambda$ in addition to $x = x_1, x_2, \ldots, x_N$ and define a new system of equation $\mathbf{h}(\mathbf{x}, \lambda) = \mathbf{0}$ in $N + 1$ variables.This mapping $\mathbf{h}$ is called the homotopy mapping. The algorithms used for the solution of above problem are classified into two, one predictor-corrector algorithms and the other piecewise linear algorithm. However, these curve tracing algorithms are not widely used in practical applications because of many reasons. One of the reasons is that the theory and the programming of these algorithms seem to be difficult for practical designers and scientists who are not familiar with the curve tracing algorithms. Here, a sphere based algorithm is used for the parametric continuation. Equations (27) and (38) are of size $N \times N$. Considering the excitation frequency ω as the continuation parameter and adding the variable $\Delta\omega$ to the existing N variables thus making the equation a size $N \times N+1$. $\Delta\omega$ is calculated by taking $\partial/\partial\omega$ of (27) and (40). One more equation is added to these existing N equations

in $N+1$ variables, which is the equation of a hypersphere given by

$$(x_1-c_1)^2+(x_2-c_2)^2+\cdots+(x_N-c_N)^2=r^2, \quad (48)$$

where r is the user given radius for the continuation and c is the coordinates of the center of the sphere. In this paper, a previous converged point is taken as the center. This makes the size of the equations of motion $(N+1)\times(N+1)$. Thus, the regular matrix inverse/iteration methods can be used. Thus, the final Jacobian form of (27) and (40) will be given by

$$\begin{bmatrix} \mathbf{dY}_{11} & \mathbf{dY}_{12} \\ \mathbf{dY}_{21} & \mathbf{dY}_{22} \end{bmatrix} \begin{Bmatrix} \Delta\tilde{\mathbf{x}} \\ \Delta\omega \end{Bmatrix} = \begin{Bmatrix} \mathbf{R}(\tilde{x}) \\ R'^2 \end{Bmatrix}, \quad (49)$$

where

$$\mathbf{dY}_{11}=\frac{\partial(\mathbf{Y}\hat{\mathbf{x}}+\hat{\mathbf{f}}_{\mathrm{p}}(\hat{\mathbf{x}})+\hat{\mathbf{f}}(\hat{\mathbf{x}})-\hat{\mathbf{F}})}{\partial\tilde{\mathbf{x}}},$$

$$\mathbf{dY}_{12}=\frac{\partial(\mathbf{Y}\hat{\mathbf{x}}+\hat{\mathbf{f}}_{\mathrm{p}}(\hat{\mathbf{x}})+\hat{\mathbf{f}}(\hat{\mathbf{x}})-\hat{\mathbf{F}})}{\partial\omega},$$

$$\mathbf{dY}_{21}=\frac{\partial((x_1-c_1)^2+(x_2-c_2)^2+\cdots+(x_N-c_N)^2-r^2)}{\partial\tilde{\mathbf{x}}},$$

$$\mathbf{dY}_{22}=\frac{\partial((x_1-c_1)^2+(x_2-c_2)^2+\cdots+(x_N-c_N)^2-r^2)}{\partial\omega},$$

and $R'^2=((x_1-c_1)^2+(x_2-c_2)^2+\cdots+(x_N-c_N)^2-r^2)$.

3.7 Stability

As the entire solution curve is traced, stability of the solution is also important. The stability can be found in many ways and in this paper the method suggested by Rook [23] is used for the stability calculation with TVM and Groll and Ewins [30] for HBM. In this method, perturbation is assumed to be periodic and the perturbed equation is transformed to form a quadratic eigenvalue problem. Such an eigenvalue problem is solved and the real part of the resulting eigenvalues determine the local stability of the solution. If all the eigenvalues are negative, the system is considered to be asymptotically stable, and if at least one of them is positive the system is unstable.

3.8 Solution routines

In general, the Gauss elimination method (LU Decomposition) is used for the solution of the linear system. The least square solvers based on QR and SVD can be used for solving square linear system. From the point of view of number of operations, Gauss elimination is the best way to solve a square linear system $Ax=b$ by reducing to an equivalent triangular system, so that it can be solved easily. The solution to the original problem is found by a two step substitution process. If the size of the matrix is N, then it takes $2N^3/3$ operations. When the condition number of the matrix is very high, the Gaussian updates will be erroneous and lead to wrong results.

QR Decomposition the matrix A of size $M\times N$ is factored into $A=QR$ where $Q\in\mathcal{R}^{M\times M}$ is orthogonal and $R\in\mathcal{R}^{M\times N}$ is upper triangular.When the matrix A becomes ill-conditioned, the QR gives an added advantage over the Gauss elimination in terms of the reliability of solution. In the case of nonlinear systems, this factor is very important. If the size of the matrix is N, then it takes $4N^3/3$ operations.

SVD Decomposition of a matrix A is defined as follows. Let $U_\Sigma^T B V_\Sigma=\Sigma=\mathrm{diag}(\sigma_1,\sigma_2,\ldots,\sigma_n)\in\mathcal{R}^{m\times n}$, and by defining $U=U_B U_\Sigma$ and $V=V_B V_\Sigma$, so that $U^T AV=\Sigma$ is the SVD of A. In case of ill-conditioning, the orthogonal methods give an added measure of reliability. SVD is superior for producing meaningful solutions to a nearly singular system. The number of operations involved in carrying out an SVD is $12N^3$ for a matrix of size N.

In the Powell Hybrid (PH) method, the choice of the step correction is carried out as a convex combination of the Newton and scaled gradient directions, and updation of the Jacobian is carried out by the rank-1 method of Broyden. The choice of the correction guarantees (under reasonable conditions) global convergence for starting points far from the solution and a fast rate of convergence. The Jacobian is calculated at the starting point, but it is not recalculated until the rank-1 method fails to produce satisfactory progress. In this method, a line search algorithm is used for accepting and rejecting the step length. This method seems to be more robust even though the number of operations are higher. Additional computational burden is balanced by the Broyden update of the Jacobian.

4 Validation

Dai et al. [31] used a piecewise-constant technique (P-T) for the analysis of 2 DOF nonlinear system with

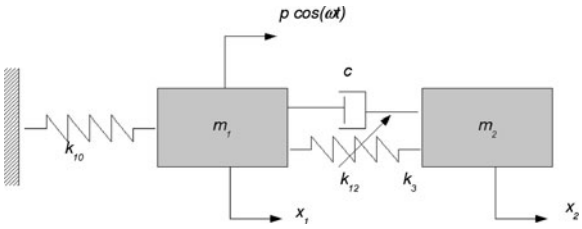

Fig. 5 Validation model (2 DOF)

a 1:3 internal resonance. Two nonlinear oscillation systems with quadratic and cubic nonlinearities are solved to demonstrate the applications of the method. The numerical methods proposed in this paper are validated using the 2 DOF cubic nonlinear model from the paper by Dai et al. [31]. The model used is as shown in Fig. 5. The governing equations of motion are given by

$$\begin{bmatrix} m_1 & 0 \\ 0 & m_2 \end{bmatrix} \begin{Bmatrix} \ddot{x}_1 \\ \ddot{x}_2 \end{Bmatrix} + \begin{bmatrix} c & -c \\ -c & c \end{bmatrix} \begin{Bmatrix} \dot{x}_1 \\ \dot{x}_2 \end{Bmatrix} + \begin{bmatrix} k_{10}+k_{12} & -k_{12} \\ -k_{12} & k_{12} \end{bmatrix} \begin{Bmatrix} x_1 \\ x_2 \end{Bmatrix} + \begin{Bmatrix} k_3(x_1-x_2)^3 \\ -k_3(x_1-x_2)^3 \end{Bmatrix} = \begin{Bmatrix} p\cos(\omega t) \\ 0 \end{Bmatrix} \tag{50}$$

with the parameters mentioned in the paper (51) becomes

$$\begin{bmatrix} 1.2 & 0 \\ 0 & 1 \end{bmatrix} \begin{Bmatrix} \ddot{x}_1 \\ \ddot{x}_2 \end{Bmatrix} + \begin{bmatrix} 0.2 & -0.2 \\ -0.2 & 0.2 \end{bmatrix} \begin{Bmatrix} \dot{x}_1 \\ \dot{x}_2 \end{Bmatrix} + \begin{bmatrix} 18.68 & -2 \\ -2 & 2 \end{bmatrix} \begin{Bmatrix} x_1 \\ x_2 \end{Bmatrix} + \begin{Bmatrix} 0.02(x_1-x_2)^3 \\ -0.02(x_1-x_2)^3 \end{Bmatrix} = \begin{Bmatrix} p\cos(\omega t) \\ 0 \end{Bmatrix} \tag{51}$$

and for three different values of p such as 1, 5, and 10.

4.1 Validation results

The validation is done with full TVM (without mode superposition and master-slave partition) and with numerical integration. As the model is two DOF, both the DOF are compared for the validation, and are shown in Figs. 6 and 7. From the figures, it is clear that the present method agree very well with Dai et al. [31] paper. The method described by Dai et al. does not have continuation algorithm, and hence in the paper solution curves along jump are not traced. In the present method, continuation is used to trace the solution curve along the jumps.

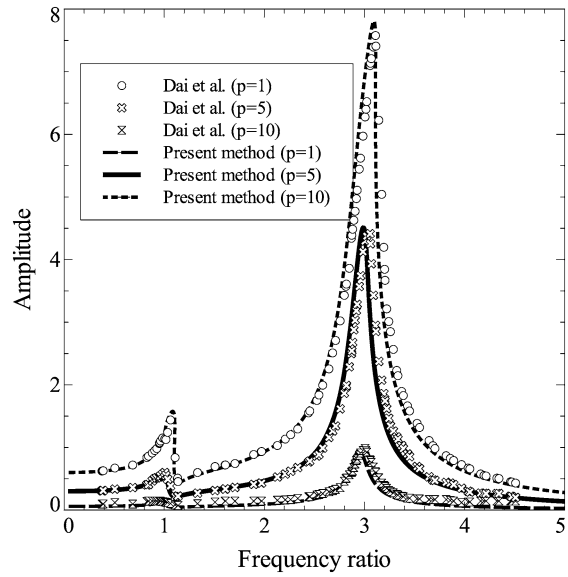

Fig. 6 Validation model, 1st DOF comparison

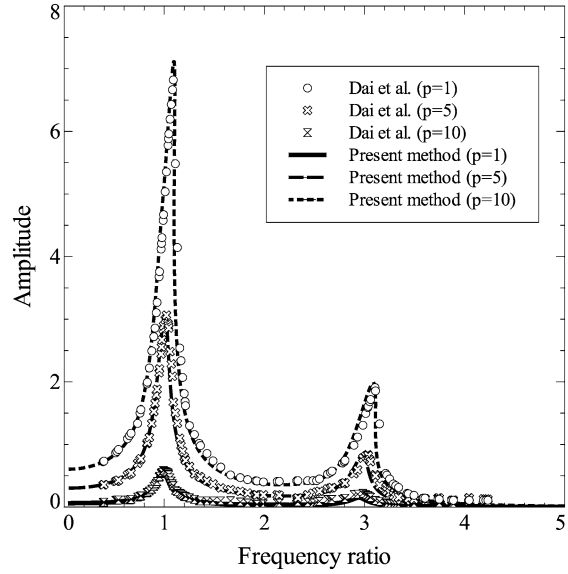

Fig. 7 Validation model, 2nd DOF comparison

5 Results

The full models were considered only for the 3 DOF discrete system. The 3 DOF discrete system is solved using numerical integration (without continuation), HBM, and TVM with continuation. The beam axial and beam bending is solved using numerical integration (without continuation) and harmonic balance and time variational method with mode superposition (of linear model). In the mode superposition methods, the first two modes of the slave subsystem are used for model reduction. The convergence due to more number of modes is evaluated for the linear case. The influence of higher modes is insignificant because of well-separated eigenvalues, for both axial and bending problems. Dynamic condensation is implemented using only two DOF as master (where the external force is applied and the nonlinear DOF) and the rest as slave DOF. Here, the frequency dependent dynamic flexibility matrix of the slave system is evaluated for every frequency. HBM is applied to the condensed model using component mode synthesis. The component mode synthesis is implemented with TVM, though resulting slave inverse is not analytically evaluated as in the case of HBM. Hence, for every iteration, matrix inversion is carried out. Though the Jacobian from TVM is sparse, in the present paper, the sparsity is not exploited. In component mode synthesis, the last element is considered as the nonlinear substructure (i.e., master subsystem) and the other elements are assumed to be in the slave subsystem which is linear. This reduced set of equations are solved using HBM as well as TVM. In both methods, the solution as well as the external load vector is assumed to be periodic. Hence, these methods will not predict the aperiodic responses which can occur in a nonlinear system. For HBM, 5 harmonics are considered, while for TVM 32 sampling points are considered. Plotted magnitudes are displacements of the corresponding nonlinear DOF.

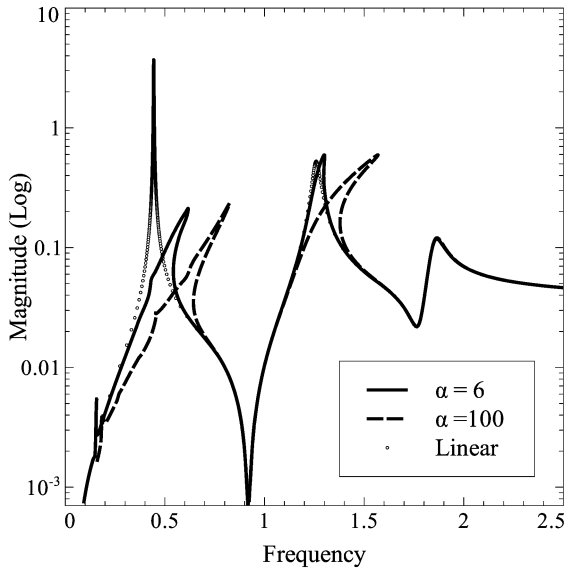

Fig. 8 3 DOF Model 1 effect of nonlinear stiffness

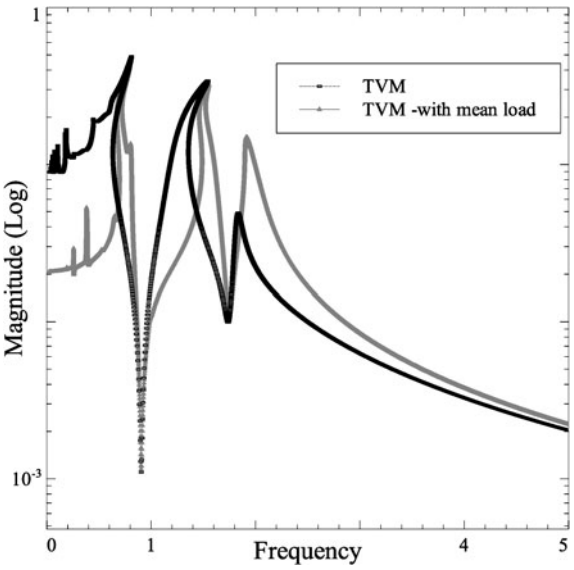

Fig. 9 3 DOF Model 1 effect of mean load

5.1 3-DOF discrete system

Three different nonlinear stiffness (α) values are used for the dynamic response analysis of the system. Effect of mean load is also studied by applying a mean load in addition to the harmonic excitation. The effect on increase in the nonlinear stiffness on the system (Fig. 1) response is shown in Fig. 8. Figure 9 shows the effect of mean load on the dynamic response of the system shown in Fig. 1. The effect of mean load is evident from the figure that the curve initially softens (bend backwards) and then stiffens (bend forward). In the case of a system with no mean load, the system exhibits hardening behavior with a positive nonlinear stiffness value. Since the nonlinear values used are very high compared to the linear stiffness value, the response curve has sharp turning points. In the case of the numerical integration process with out continua-

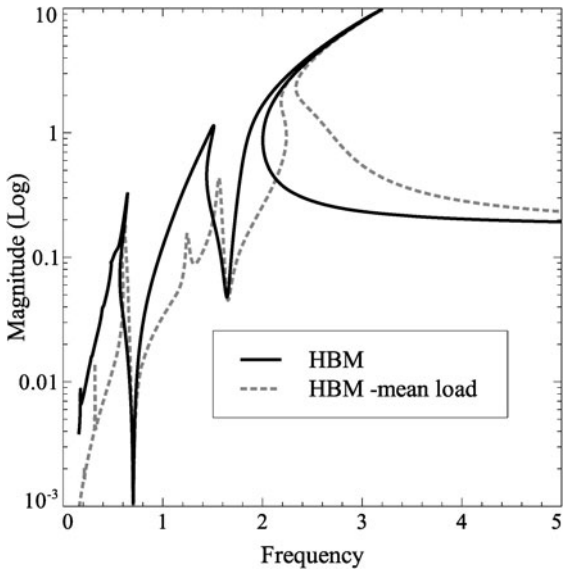

Fig. 10 3 DOF Model 2 effect of mean load

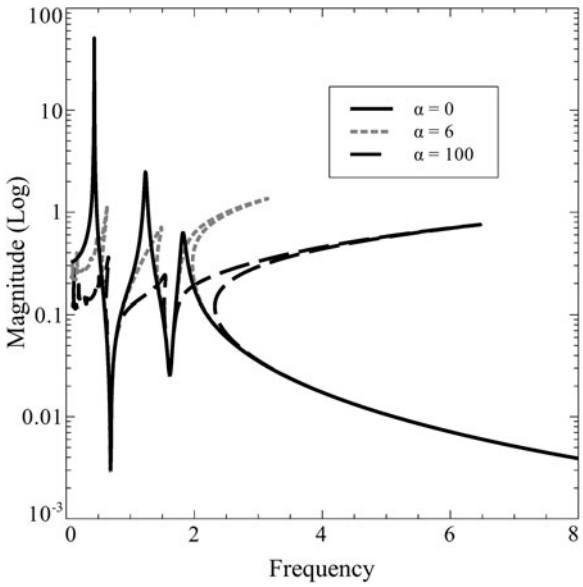

Fig. 11 3 DOF Model 2 effect of nonlinear stiffness

tion, it will not be possible to trace these paths. The present algorithm is very efficient in tracing this curve with sharp turning points. The linear response of the system shown in Fig. 2 is same as that of the system shown in Fig. 1. In Fig. 10, the effect of mean load is shown for the system shown in Fig. 2 when the nonlinear stiffness value is $\alpha = 6$. The solution is sought using HBM. The behavior of the system is observed to be the same as that of in the previous case, and in this case the forward frequency shifting is very evident due to the fact that the movement of the 3rd mass is arrested in the presence of mean load, and hence increasing the over all system stiffness, where as in the case of the first system the 3rd mass is free to move, and hence the over all stiffness increase will be minimum. The effect of increase in the nonlinear stiffness value is shown in Fig. 11. The forward leaning of the response curve is increasing as the stiffness increases and the response becomes more sharper. But the frequency shifting is not evident due to the absence of mean load.

5.2 Beam axial vibration

HBM and TVM methods are used in the reduced model with mode superposition method, dynamic substructuring, and component mode synthesis based dynamic substructuring approach. Two modes were used for representing the slave system and 5 harmonics

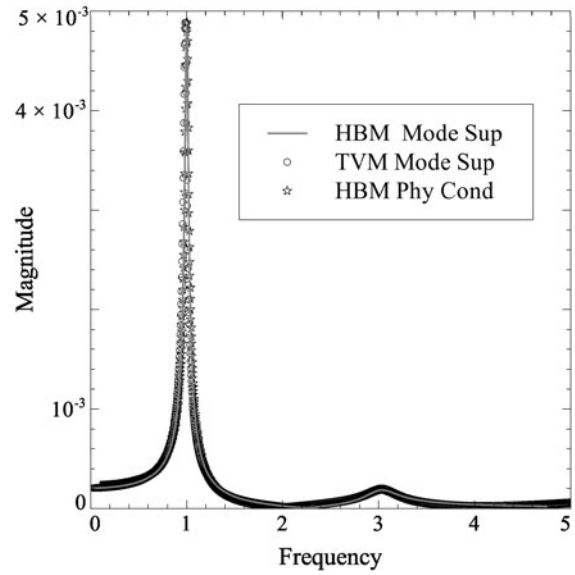

Fig. 12 Beam axial mode linear comparison

are included in HBM, and 32 points were used for the TVM. Figure 12 displays the results obtained by using the different methods described in this paper. The X-axis shows a normalized frequency with respect to the fundamental frequency of the system and Y-axis shows the amplitude. The linear results show very good agreement with each other. This validates the methodology. The base nonlinear stiffness value is

Table 4 HBM, TVM Model Details

Model	FM	MS	PC		CM		
	DOF	# of Modes (m)	Master	Slave	Master	Slave	# of Slave modes (l)
Beam Axial	10	2	2	8	2	8	2
Beam Bending	20	2	2	18	4	16	2

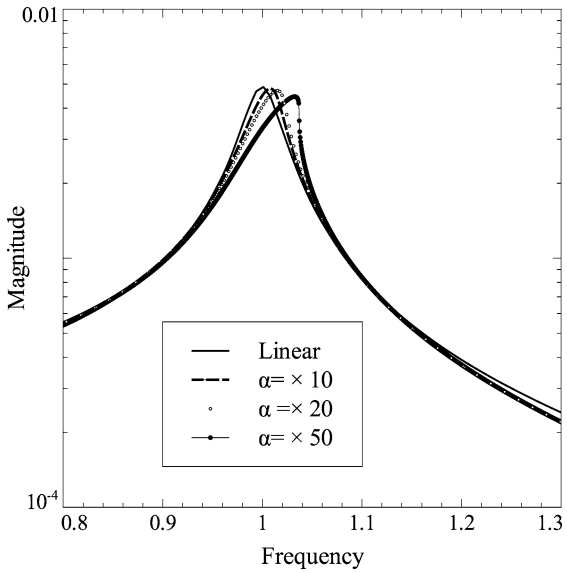

Fig. 13 Effect of increase in nonlinear stiffness

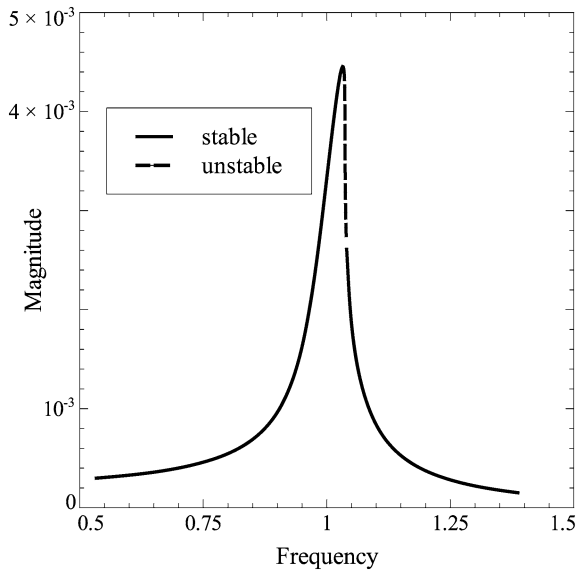

Fig. 14 Stability for beam axial $\alpha = 50$

taken as 100 times that of the largest coefficient in the linear stiffness matrix and the nonlinearity is increased from this value. Figure 13 displays the response of the system with different nonlinear stiffness values. The forward bending of the response curve is evident as the nonlinear stiffness increases. The numerical convergence properties are explained later in the paper. Table 4 consolidates the model after reduction. Stability of the solution is carried out as shown in Fig. 14.

5.3 Beam bending

Here, also, the model size is reduced using mode superposition method and component mode synthesis based dynamic substructuring approach. For both, the methods master-slave partition-based dynamic condensation is also carried out. Here, the boundary DOF will be 2 because beam has one vertical DOF and one rotational DOF at the boundary. Figure 15 shows the comparison between mode superposition based HBM, TVM, component mode based dynamic substructuring HBM method, and with numerical integration. All these methods shows very good agreement with each other. Here, also the graphs are plotted with normalized frequency on the X-axis and amplitude on the Y-axis. In the logarithmic graphs, even though the scale is logarithm actual values are marked on the Y-axis. Here, the base nonlinear stiffness is assumed to be the stiffness of the clamped-pinned beam and the nonlinear stiffness ($\alpha = 1\,300\,800$) is varied as multiple of the same. In Fig. 16, the HBM with the mode superposition and the component mode synthesis results are compared and an excellent agreement is observed. In the same figure, the subharmonic responses can be observed which is characteristic behavior of the nonlinear system. In Fig. 17, the effect of mean load on the nonlinear response is plotted and the frequency shifting is observed and peak amplitude is reduced. This due to the fact that the boundary of the cantilever is now not free to move as freely as the case with out the mean load, thereby increasing the overall stiffness which causes the frequency shift and the reduction in

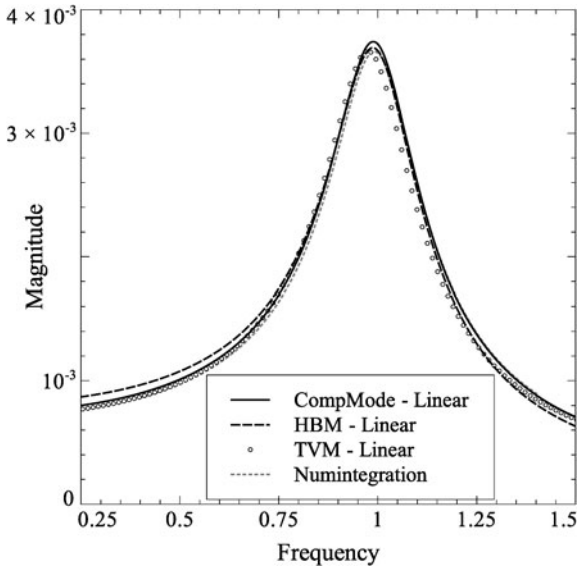

Fig. 15 Beam bending linear comparison

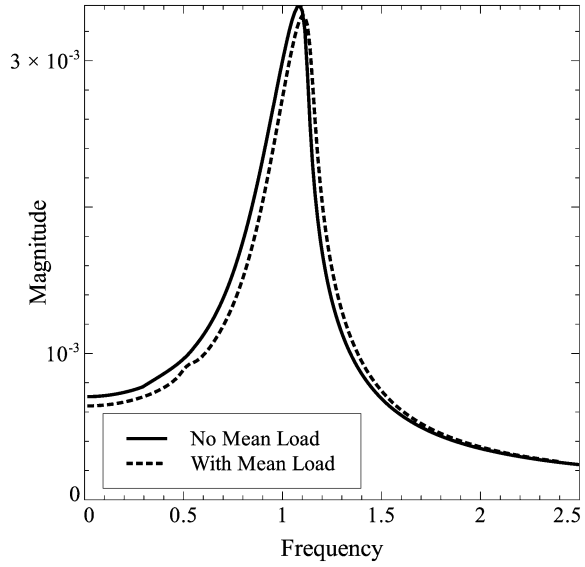

Fig. 17 Beam bending effect of mean load

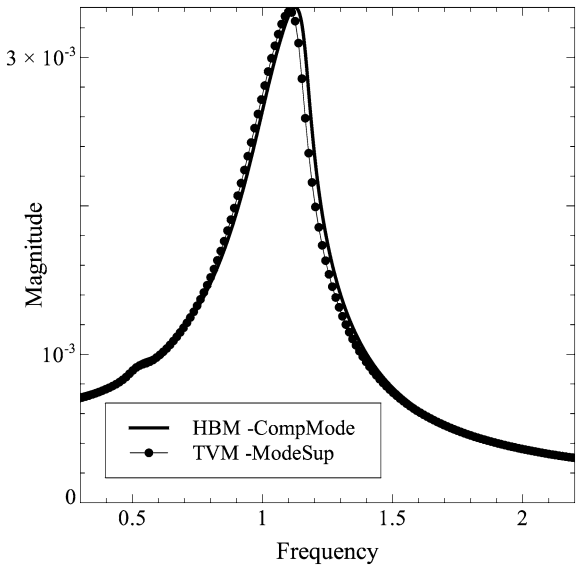

Fig. 16 Beam bending nonlinear model comparison

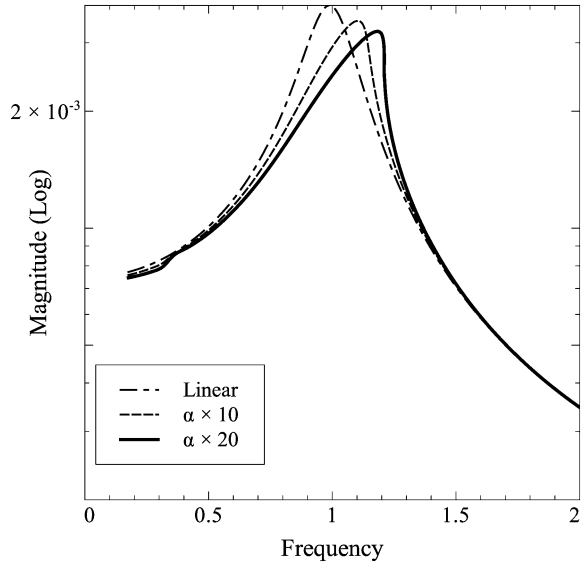

Fig. 18 Beam bending effect of nonlinear stiffness

the overall amplitude. Figure 18 shows the effect of the nonlinear stiffness in the response characteristics. The forward bending of the response curve is increased by increasing the stiffness. When the nonlinear stiffness is as high as 50 times, all the solution techniques started to diverge. Stability of the solution is carried out as shown in Fig. 21.

The effect of kept modes on the dynamic response is studied using the refined mesh (20 elements model). The number of slave kept modes is varied from 1 to 10. The results are shown in Fig. 20, from which it is clear that increasing the number modes beyond 2 has no effect on the system response (The zoomed view shows a difference but the difference in peak is less than 0.1%). This is due to the fact that even though the system is nonlinear, response near the first mode of the linear system is only considered in the analysis and the higher mode frequencies are well separated. It is ex-

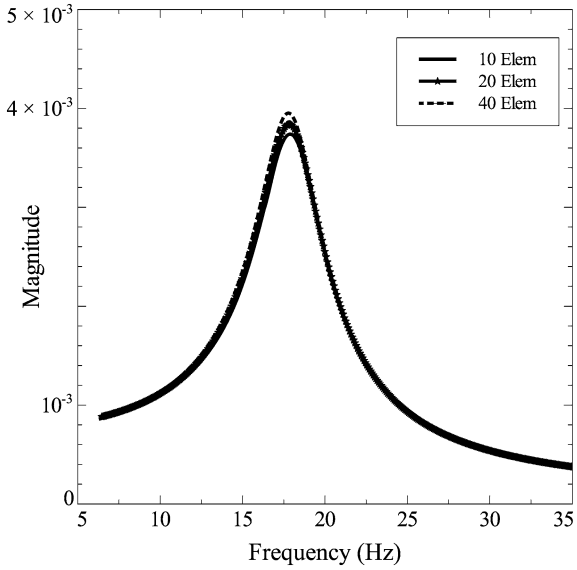

Fig. 19 Convergence with number of elements

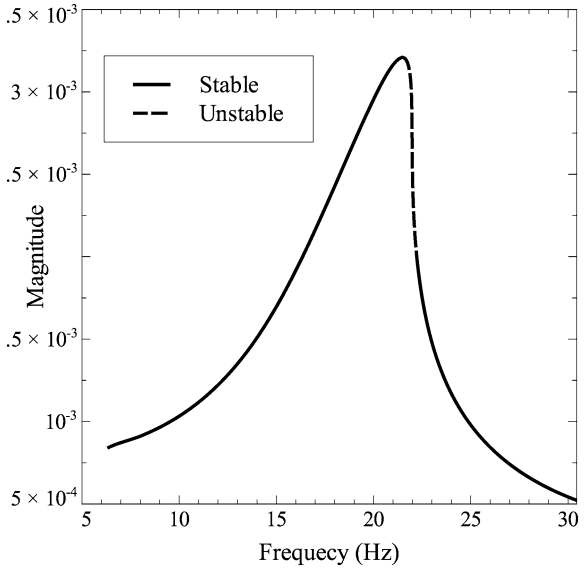

Fig. 21 Stability for beam bending $\alpha = 20$

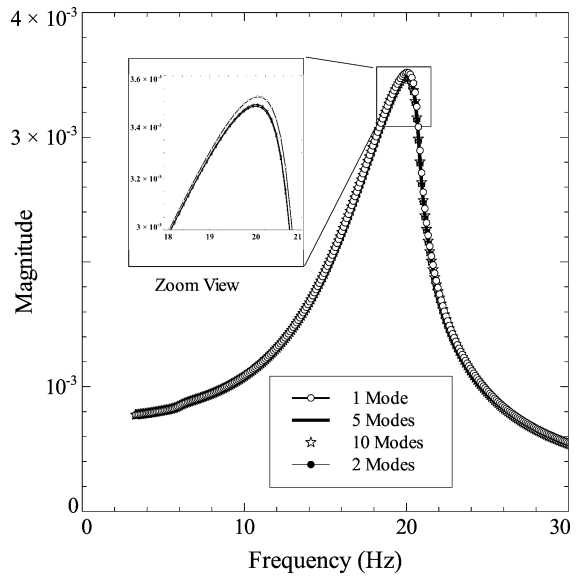

Fig. 20 Beam bending effect of kept modes; 20 elements, 40 DOF ($\alpha \times 10$)

pected to have more effects as the frequency of interest changes to the higher modes of the linear system. Figure 19 shows the results of mesh convergence study. Table 4 consolidates the model after reduction.

5.4 Beam parametric excitation

Component mode-based dynamic substructuring with HBM is used for solving the problem. First, two modes of the slave system are included in the solution with the DOF associated with the time-varying stiffness being the master system. The system is subjected to an external excitation with mean load along with the parametric excitation. Sixteen harmonics are included to capture the higher order response components. Parametric excitation coefficient α is varied from 0.1 to 0.8 and the results are shown in Fig. 22. As the parametric excitation term has a frequency 2ω, all the even frequency components are dominant, especially those close to one-half the system natural frequencies. At lower α values, the effect of higher order components is not clearly visible; they become dominant as α increases. At $\alpha = 0.8$, the amplitude at $\omega_1/2$ is dominant compared to that at ω_1. So for a parametrically excited system, in the presence of mean load, higher vibration levels can occur even at frequencies other than the resonance frequency. Stability of the solutions can be calculated as outlined in Sect. 3.7.

5.5 System with internal resonance

Component mode-based dynamic substructuring with HBM is again used for the solution. The system is partitioned into a 7 DOF slave system, 1 boundary DOF,

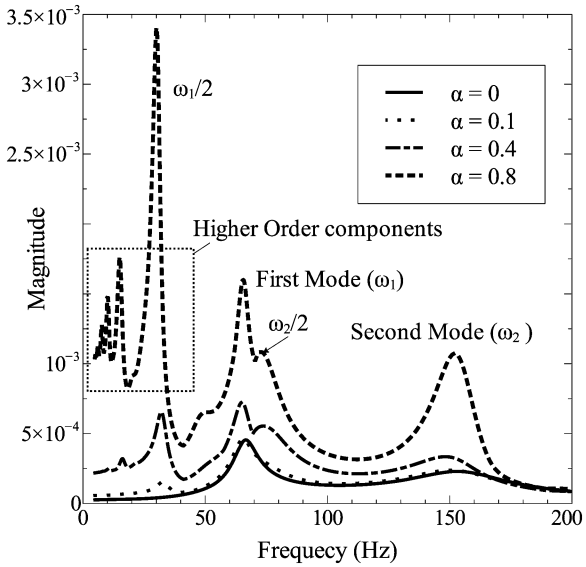

Fig. 22 Beam parametric excitation

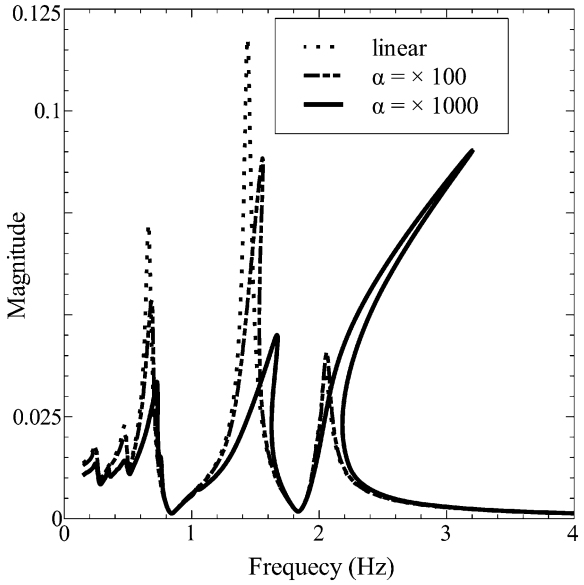

Fig. 23 MDOF system with internal resonance

and 1 DOF master system. The full system undamped natural frequencies are $\{0.26, 0.49, 0.66, 1.44, 1.95, 1.98, 1.99, 2.04, 2.07\}^T$ Hz. There is a near 1:1 internal resonance between the fifth and sixth natural frequencies with $\omega_6/\omega_5 = 1.005$. The slave system undamped natural frequencies are $\{0.29, 0.51, 1.24, 1.95, 1.98, 2.00, 2.06\}^T$ Hz. One can clearly identify that there is a near 1:1 internal resonance between the fifth and the sixth slave system natural frequencies. All seven modes of the slave system are used in the analysis to include the internal resonance effect. The undamped natural frequencies of the final assembled system are the same as that of the full system. For this example, the dynamics of the system are captured without any approximation. Figure 23 shows the response of the system. As in the case of 3 DOF system, forward bending can be observed in this system as the nonlinear stiffness increases. Figure 24 shows a zoomed view of the response in the low frequency range, to show the presence of $\omega/3$ components.

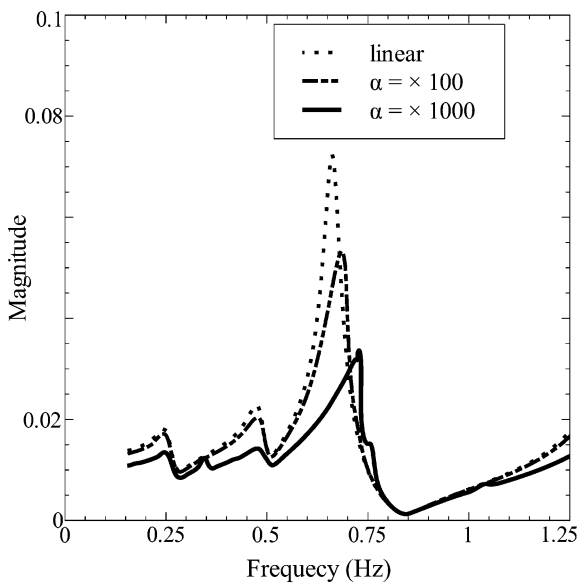

Fig. 24 Zoomed view of internal resonance

5.6 Numerical methods convergence

The numerical methods used for the solution methods are taken from the numerical library SLATEC [32]. Tables 6, 7 and 8 consolidate the convergence properties obtained for the different cases tried for the beam axial and beam bending problems. 3 DOF discrete systems are not listed in the comparison table because of the fact that the condition number of the matrix involved is small as the matrix elements are of the same order. In the case of the beam axial, the elements of the matrix will be similar because the beam is having only one DOF per node. In the case of beam bending, matrix elements will not be of the same order because of the presence of the rotation along with the translational motion. This may be the reason for the

convergence of system with a higher nonlinear stiffness with TVM in the case of beam axial motion. The TVM along with the Powell hybrid method showed a good convergence property for both the problems. This may be due to the fact that the analytical Jacobian is used only in the first iteration and for the rest of the iterations Broyden updates are used. In this paper, the sparse structure of the Jacobian of the TVM method is not utilized. The use of sparse routines may reduce the solution time.

The HBM/TVM method along with mode superposition show poor convergence. This is due to the fact that modal transformation of the nonlinear forces spreads the nonlinearity to all modal coordinates. The number of modes and the interaction between the modes required for the actual representation of the nonlinear force may not be sufficient. Hence, the increase in nonlinear stiffness causes poor convergence. The global nature of the basis functions cause the Broyden update of the Jacobian to be poor for HBM, while for TVM local support basis functions helps the Broyden update and hence aids convergence of the Powell hybrid method. This is due to the fact that Broyden update in the case of HBM is done on the Fourier coefficients of the modal coordinates, and then transformed back to the physical coordinates. Hence, there are two levels of approximation. In the case of TVM as the function is already in the time domain only, the modal transformation is required, and hence Broyden approximation yields better convergence properties.

For component mode synthesis-based dynamic substructuring, the nonlinear DOF and the boundary DOF are kept back in the physical coordinates and the linear slave system is transformed into the modal space. The slave inverse which needs to be carried out for every iteration is performed using an analytical inverse calculation. Hence, a better convergence is observed in case of HBM with the component mode based dynamic substructuring. The component mode based dynamic substructuring shows better convergence properties for the beam case with TVM though analytical expression of slave dynamic flexibility matrix does not lead to a unique structure, and in most of the cases it will be sparse. In the case of regular dynamic condensation, convergence is the same as that of the component mode-based dynamic condensation; though it takes more solution time. This is expected because the slave dynamic flexibility matrix is frequency dependent and it is evaluated for each iteration by an inverse. This can be reduced by doing a Sherman–Morrison approximation type inverse update. Standard preconditioning technique for the Jacobian using the maximum value of each row does not show much difference in convergence characteristics of the system in all these cases. Hence, to improve the convergence, some other preconditioning techniques have to be adopted.

Computational effort required for HBM and TVM with dynamic condensation is high, because of the large size of slave dynamic flexibility matrix. For the component mode based substructuring, let l be the number of slave retained modes and n be the number of Fourier/TVM coefficients (If $nhar$ is the number of harmonics considered, then n will be equal to $2nhar + 1$ for HBM and will be equal to the sampling points in the case of TVM). Then size of slave flexibility matrix will be of $l \times n$; so in the case of HBM will be saving $2(l \times n)^3$ matrix multiplications as the inverse calculation is eliminated. This requires a storage of $2(l \times n)^2$ as full storage is required, while if we use the sparse structure for TVM that will require only a storage of $O(l \times n)$, and by proper selection of the inverse routine the multiplications can also be of the same order. Hence, both the methods applied along with dynamic condensation and component mode will be computationally efficient. Table 5 compares the computational requirements for the HBM for dynamic condensation and dynamic condensation with component mode with out analytical inverse and dynamic condensation with component mode with analytical inverse. Let nh be the number of harmonics, ns is the total number of slave DOF and m the number of included modes of slave system. Let $N_1 = (ns \times (2nh + 1))$ and $N_2 = (m \times (2nh + 1))$.

Table 5 Number of multiplications involved in computation

	PC	HBM CM numerical inverse	HBM CM analytical inverse
Total Size	$N_1 \times N_1$	$N_2 \times N_2$	$N_2 \times N_2$
Storage	$N_1 \times N_1$	$N_2 \times N_2$	$N_2 \times N_2$
# of Operations (LU)	$2N_1^3/3$	$2N_2^3/3$	N_2

Table 6 Convergence comparison between different methods

Model	α	HBM MS				TVM MS			
Beam Axial	2 868 000 000	LU	QR	SVD	PH	LU	QR	SVD	PH
Linear	$\times 0$	C	C	C	C	C	C	C	C
Mean Load 0	$\times 10$	C	C	C	C	C	C	C	C
Mean Load 1E4	$\times 10$	C	C	C	C	C	C	C	C
Mean Load 0	$\times 20$	D	D	D	D	D	D	D	C
Mean Load 1E4	$\times 20$	D	D	D	D	D	D	D	C
Mean Load 0	$\times 50$	D	D	D	D	D	D	D	C
Beam Bending	1 300 800								
Linear	$\times 0$	C	C	C	C	C	C	C	C
Mean Load 0	$\times 10$	D	D	D	D	D	D	D	C
Mean Load 10	$\times 10$	D	D	D	D	D	D	D	C
Mean Load 0	$\times 20$	D	D	D	D	D	D	D	C
Mean Load 10	$\times 20$	D	D	D	D	D	D	D	C
Mean Load 0	$\times 50$	D	D	D	D	D	D	D	D

C—solution converged; D—solution diverged

Table 7 Convergence comparison between different methods 2

Model	α	HBM PC				TVM PC			
Beam Axial	2 8 68 000 000	LU	QR	SVD	PH	LU	QR	SVD	PH
Linear	$\times 0$	C	C	C	C	C	C	C	C
Mean Load 0	$\times 10$	C	C	C	C	C	C	C	C
Mean Load 1E4	$\times 10$	C	C	C	C	C	C	C	C
Mean Load 0	$\times 20$	C	C	C	D	C	C	C	C
Mean Load 1E4	$\times 20$	C	C	C	D	C	C	C	C
Mean Load 0	$\times 50$	C	C	C	D	C	C	C	C
Beam Bending	1 300 800								
Linear	$\times 0$	C	C	C	C	C	C	C	C
Mean Load 0	$\times 10$	C	C	C	C	C	C	C	C
Mean Load 10	$\times 10$	C	C	C	C	C	C	C	C
Mean Load 0	$\times 20$	C	C	C	D	C	C	C	C
Mean Load 10	$\times 20$	C	C	C	D	C	C	C	C
Mean Load 0	$\times 50$	D	D	D	D	D	D	D	D

C—solution converged; D—solution diverged

6 Conclusion

In the present paper though a cubic nonlinearity has been considered (continuous and differentiable), convergence difficulties appear when the nonlinearity becomes very strong. Model order reduction techniques along with HBM and TVM are studied to handle a large system with strong localized nonlinearities. The convergence properties of different solution techniques have been investigated. The major contribution of this paper is the analytical calculation of the slave dynamic flexibility matrix due to judicious par-

Table 8 Convergence comparison between different methods 3

Model	α	HBM CM				TVM CM			
Beam Axial	2 868 000 000	LU	QR	SVD	PH	LU	QR	SVD	PH
Linear	×0	C	C	C	C	C	C	C	C
Mean Load 0	×10	C	C	C	C	C	C	C	C
Mean Load 1E4	×10	C	C	C	C	C	C	C	C
Mean Load 0	×20	C	C	C	D	C	C	C	C
Mean Load 1E4	×20	C	C	C	D	C	C	C	C
Mean Load 0	×50	C	C	C	D	C	C	C	C
Beam Bending	1 300 800								
Linear	×0	C	C	C	C	C	C	C	C
Mean Load 0	×10	C	C	C	C	C	C	C	C
Mean Load 10	×10	C	C	C	C	C	C	C	C
Mean Load 0	×20	C	C	C	C	C	C	C	C
Mean Load 10	×20	C	C	C	C	C	C	C	C
Mean Load 0	×50	D	D	D	D	D	D	D	D

C—solution converged; D—solution diverged

tition of the slave master system and arrangement of the Fourier coefficients. This leads to a better convergence rate as well as reduced solution time. The hypersphere-based continuation uses regular matrix inverse/iteration routines which are more robust than the pseudo inverse routines. The use of QR and SVD methods do not prove to be of much use in enhancing the convergence rate for both HBM and TVM. This may be due to the Jacobian being square because of hypersphere-based continuation. LU decomposition can be used with a better rate of convergence for the component mode-based dynamic condensation method. The Powell hybrid method along with mode superposition shows good convergence properties only for the beam axial case. In that case, the elements of the stiffness and mass matrices are of same order, and hence it will not have a large condition number.

Convergence of a nonlinear problem depends on the machine precision. Even for a continuous nonlinearity, high condition number of the Jacobian matrix, demands better than machine precision for convergence. This limit depends on the technique associated with the solution. From this perspective, the component mode synthesis based approach is better, since only the lower order modes are used, leading to lower condition numbers. In addition, this technique requires one less matrix inverse which adds to its robustness. For the TVM method, sparsity of the Jacobian structure has to be utilized further to enhance the convergence and reduce the solution time.

The regular dynamic condensation also has a good convergence rate. The advantage of this method is that the slave system is not approximated as it is not transformed into the modal space. The disadvantage is its requirement of computing the slave dynamic flexibility matrix which involves an inverse calculation for every iteration, leading to higher condition numbers and possible convergence issues.

There are a few limitations for using the described method in the paper. If gyroscopic effects are present in the slave system, then one will have to use frequency dependent mode shapes for transforming the system. But if the gyroscopic effects are only at discrete locations, then these locations can be moved into the master system and the procedure proposed in this paper can be applied. In all these cases, the damping is assumed to be proportional for analytical inverse calculation.

Appendix A: Dynamic substructuring

To include the parametric continuation along with the master slave reduction, the derivative of (31) with respect to the excitation frequency ω is needed. The

equations given below will give the corresponding differentiation matrices.

$$\frac{\partial(.)}{\partial\omega} = \frac{\partial(\mathbf{Y}_{\mathrm{mm}} - \mathbf{Y}_{\mathrm{ms}}\mathbf{Y}_{\mathrm{ss}}^{-1}\mathbf{Y}_{\mathrm{sm}})}{\partial\omega}\tilde{\mathbf{x}}_{\mathrm{m}}. \tag{52}$$

The differentiation is given by

$$\frac{\partial(\mathbf{Y}_{\mathrm{mm}} - \mathbf{Y}_{\mathrm{ms}}\mathbf{Y}_{\mathrm{ss}}^{-1}\mathbf{Y}_{\mathrm{sm}})}{\partial\omega} = \frac{\partial(\mathbf{Y}_{\mathrm{mm}})}{\partial\omega} - \left(\frac{\partial(\mathbf{Y}_{\mathrm{ms}})}{\partial\omega}\mathbf{Y}_{\mathrm{ss}}^{-1}\mathbf{Y}_{\mathrm{sm}} + \mathbf{Y}_{\mathrm{ms}}\frac{\partial(\mathbf{Y}_{\mathrm{ss}}^{-1})}{\partial\omega}\mathbf{Y}_{\mathrm{sm}} + \mathbf{Y}_{\mathrm{ms}}\mathbf{Y}_{ss^{-1}}\frac{\partial(\mathbf{Y}_{\mathrm{sm}})}{\partial\omega}\right). \tag{53}$$

which requires $\frac{\partial\mathbf{Y}_{\mathrm{ss}}^{-1}}{\partial\omega}$, and is calculated as follows:

$$\frac{\partial\mathbf{Y}_{\mathrm{ss}}^{-1}}{\partial\omega} = -\mathbf{Y}_{\mathrm{ss}}^{-1}\frac{\partial\mathbf{Y}_{\mathrm{ss}}}{\partial\omega}\mathbf{Y}_{\mathrm{ss}}^{-1}. \tag{54}$$

Appendix B: Dynamic substructuring with component mode

Derivative of the (34) with respect to the excitation frequency ω is required. The following equations give the corresponding differentiation matrices:

$$\frac{\partial(.)}{\partial\omega} = \frac{\partial(\mathbf{Y}_{\mathrm{mm}} - \mathbf{Y}_{\mathrm{ms}}\mathbf{Y}_{\mathrm{ss}}^{-1}\mathbf{Y}_{\mathrm{sm}})}{\partial\omega}\tilde{\mathbf{x}}_{\mathrm{m}f} + \frac{\partial(\mathbf{Y}_{\mathrm{ms}}\mathbf{Y}_{\mathrm{ss}}^{-1}\mathbf{Y}_{\mathrm{sm}})}{\partial\omega}\tilde{\mathbf{F}}_{\mathrm{s}}. \tag{55}$$

The differentiation of the first term is given by

$$\frac{\partial(\mathbf{Y}_{\mathrm{mm}} - \mathbf{Y}_{\mathrm{ms}}\mathbf{Y}_{\mathrm{ss}}^{-1}\mathbf{Y}_{\mathrm{sm}})}{\partial\omega} = \frac{\partial(\mathbf{Y}_{\mathrm{mm}})}{\partial\omega} - \left(\frac{\partial(\mathbf{Y}_{\mathrm{ms}})}{\partial\omega}\mathbf{Y}_{\mathrm{ss}}^{-1}\mathbf{Y}_{\mathrm{sm}} + \mathbf{Y}_{\mathrm{ms}}\frac{\partial(\mathbf{Y}_{\mathrm{ss}}^{-1})}{\partial\omega}\mathbf{Y}_{\mathrm{sm}} + \mathbf{Y}_{\mathrm{ms}}\mathbf{Y}_{\mathrm{ss}}^{-1}\frac{\partial(\mathbf{Y}_{\mathrm{sm}})}{\partial\omega}\right) \tag{56}$$

and the differentiation for the second term is given by

$$\frac{\partial(\mathbf{Y}_{\mathrm{ms}}\mathbf{Y}_{\mathrm{ss}}^{-1}\mathbf{Y}_{\mathrm{sm}})}{\partial\omega} = \left(\frac{\partial(\mathbf{Y}_{\mathrm{ms}})}{\partial\omega}\mathbf{Y}_{\mathrm{ss}}^{-1}\mathbf{Y}_{\mathrm{sm}} + \mathbf{Y}_{\mathrm{ms}}\frac{\partial(\mathbf{Y}_{\mathrm{ss}}^{-1})}{\partial\omega}\mathbf{Y}_{\mathrm{sm}} + \mathbf{Y}_{\mathrm{ms}}\mathbf{Y}_{\mathrm{ss}}^{-1}\frac{\partial(\mathbf{Y}_{\mathrm{sm}})}{\partial\omega}\right). \tag{57}$$

The differentiation matrix of $\mathbf{Y}_{\mathrm{mm}}$, $\mathbf{Y}_{\mathrm{sm}}$, and $\mathbf{Y}_{\mathrm{ms}}$ will be of same structure.

$$\frac{\partial(\mathbf{Y}_{..})}{\partial\omega} = 2\omega[\mathbf{M}]_{..} + [\mathbf{C}]_{..} \tag{58}$$

B.1 Harmonic balance

For HBM because of the special arrangement of coefficients and the differentiation matrix of the B_i^{-1} is given by for the ith DOF

$$\frac{\partial\mathbf{B}_i^{-1}}{\partial\omega} = \begin{bmatrix} 0 & 0 & 0 & 0 & 0 & \dots & 0 & 0 \\ 0 & dB_i^{11} & -dB_i^{12} & 0 & 0 & \dots & 0 & 0 \\ 0 & dB_i^{12} & dB_i^{12} & 0 & 0 & \dots & 0 & 0 \\ 0 & 0 & 0 & dB_i^{21} & -dB_i^{22} & \dots & 0 & 0 \\ 0 & 0 & 0 & dB_i^{22} & dB_i^{21} & \dots & 0 & 0 \\ \vdots & \vdots & \vdots & \vdots & \vdots & \ddots & \vdots & \vdots \\ 0 & 0 & 0 & 0 & 0 & \dots & dB_i^{n1} & -dB_i^{n2} \\ 0 & 0 & 0 & 0 & 0 & \dots & dB_i^{n2} & dB_i^{n1} \end{bmatrix}, \tag{59}$$

where $\Omega_{\mathrm{s}i}$ is the ith natural frequency and n is the number of harmonics.

$$DR = \left(\Omega_{si}^2 - (j\omega)^2\right)^2 + (2\zeta j\omega\Omega_{si})^2,$$

$$dB_i^{j1} = \frac{-2j^2\omega}{DR} + \frac{(\Omega_{si}^2 - (j\omega)^2)((2j\zeta\Omega_{si})^2(2\omega) - (4j^2\omega)(\Omega_{si}^2 - (j\omega)^2))}{DR^2},$$

$$dB_i^{j2} = \frac{(2j\zeta\Omega_{si}\omega)((2j\zeta\Omega_{si})^2(2\omega) - (4j^2\omega)(\Omega_{si}^2 - (j\omega)^2))}{DR^2} - \frac{2j\zeta\Omega_{si}}{DR},$$

where $n = 1, 2, 3, \ldots m$, where m is the number of terms in the Fourier expansion.

References

1. Guyan, R.J.: Reduction of stiffness and mass matrices. AIAA J. **3**, 380 (1965)
2. Leung, A.Y.T., Fung, T.C.: Linear and nonlinear substructures. Int. J. Numer. Methods Eng. **31**, 967–985 (1991)
3. Qu, Z.-Q.: Model Order Reduction Techniques with Applications in Finite Element Analysis. Springer, Berlin (2004)
4. Hurty, W.C.: Dynamic analysis of structural systems using component modes. AIAA J. **3**(4), 678–685 (1965)
5. Craig, R.R., Jr., Bampton, M.C.C.: Coupling of substructures for dynamic analysis. AIAA J. **6**(7), 1313–1319 (1968)
6. Yousef, S.: Iterative Methods for Sparse Linear Systems, 2nd edn. SIAM, Philadelphia (2003)
7. Hairer, E., Wanner, G., Norsett, S.P.: Solving Ordinary Differential Equations. I. Nonstiff Problems, vol. I. Springer, Berlin (1980)
8. Hairer, E., Wanner, G.: Solving Ordinary Differential Equations. II. Stiff and Differential-Algebraic Problems, vol. II. Springer, Berlin (1980)
9. Fung, T.C., Fan, S.C.: Mixed time finite elements for vibration response analysis. J. Sound Vib. **213**(3), 409–428 (1998)
10. Urabe, M., Reiter, A.: Numerical computation of nonlinear forced oscillations by Gelarkin's method. J. Math. Anal. Appl. **14**, 107–140 (1966)
11. Leung, A.Y.T., Chu, S.K.: Nonlinear vibration of coupled duffing oscillators by an improved incremental harmonic balance method. J. Sound Vib. **181**, 619–633 (1995)
12. Blair, B., Krousgrill, C., Farris, T.N.: Harmonic balance and continuation technique in the dynamic analysis of the Duffing's equation. J. Sound Vib. **202**, 717–731 (1997)
13. Ragothama, A., Narayanan, S.: Bifurcations and chaos in geared rotor bearing system by incremental harmonic balance method. J. Sound Vib. **226**(3), 469–492 (1999)
14. Cheung, Y.K., Chen, S.H., Lau, S.L.: Application of incremental harmonic balance method to cubic nonlinearity systems. J. Sound Vib. **140**, 273–286 (1990)
15. Feri, A.A., Dowell, E.H.: Frequency domain solutions to multi degree of freedom dry friction damped system. J. Sound Vib. **124**, 207–224 (1988)
16. Wu, J.J.: A generalized harmonic balance method for nonlinear oscillations: the sub harmonic cases. J. Sound Vib. **159**, 503–525 (1992)
17. Cameron, H., Griffin, J.H.: An alternating frequency/time domain method for calculating the steady state response of nonlinear dynamic systems. ASME J. Appl. Mech. **56**, 149–154 (1989)
18. Blankenship, W., Kahraman, A.: Steady state forced response of a mechanical oscillator with combined parametric excitation and clearance type nonlinearity. J. Sound Vib. **185**, 743–765 (1995)
19. Leung, A.Y.T., Fung, T.C.: Damped dynamic substructures. Int. J. Numer. Methods Eng. **26**, 2355–2365 (1988)
20. Borri, M., Bottasso, C., Mantegazza, C.: Basic features of the time finite element approach for dynamics. Meccanica **27**, 119–130 (1992)
21. Wang, Y.: Stick-slip motion of frictionally damped turbine airfoils: a finite element in time (fet) approach. ASME J. Vib. Acoust. **119**, 236–242 (1997)
22. Wang, Y.: A temporal finite element method for the dynamics analysis of flexible mechanisms. J. Sound Vib. **213**(3), 569–576 (1998)
23. Rook, T.: An alternate method to the alternating time-frequency method. Nonlinear Dyn. **27**, 327–339 (2002)
24. Broyden, C.G.: A new method of solving nonlinear simultaneous equations. Comput. J. **12**, 94–99 (1969)
25. Powell, M.J.D.: A hybrid method for nonlinear equations. In: Numerical Methods for Nonlinear Algebraic Equations. Gordon & Breach, New York (1988)
26. Yamamura, K.: Simple algorithms for tracing solution curves. IEEE Trans. Circuits Syst. I, Fund. Theory Appl. **40**(8), 534–540 (1993)
27. Padmanabhan, C., Singh, R.: Dynamics of a piecewise nonlinear system subject to dual harmonic excitation using parametric continuation. J. Sound Vib. **184**(5), 767–799 (1995)
28. Padmanabhan, C., Singh, R.: Analysis of periodically excited nonlinear systems by a parametric continuation technique. J. Sound Vib. **184**(1), 35–58 (1995)
29. Golub, G.H., VanLoan, C.F.: Matrix Computations, 3rd edn. Hindustan Book Agency, Gurgaon (2007)
30. Von Groll, G., Ewins, D.J.: The harmonic balance method with arc-length continuation in rotor/stator contact problems. J. Sound Vib. **241**(2), 223–233 (2001)
31. Dai, L., Xu, L., Han, Q.: Semi-analytical and numerical solutions of multi-degree-of-freedom nonlinear oscillation systems with linear coupling. Commun. Nonlinear Sci. Numer. Simul. **11**, 831–844 (2006)
32. Slatec common mathematical library. World Wide Web, July (1993)